A kinetic energy preserving FE/FV scheme on staggered non-conforming meshes for variable density flows

Jean-Claude Latché [1]
Bruno Piar [2]
Khaled Saleh [3]

[1] Institut de Radioprotection et de Sureté Nucléaire (IRSN), 13115 St-Paul-Lez-Durance, France
Email address: jean-claude.latche@irsn.fr
[2] Institut de Radioprotection et de Sureté Nucléaire (IRSN), 13115 St-Paul-Lez-Durance, France
Email address: bruno.piar@irsn.fr
[3] Institut Camille Jordan, Université Claude Bernard, Lyon I, 43 boulevard du 11 novembre 1918, 69622, Villeurbanne cedex, FRANCE
Email address: saleh@math.univ-lyon1.fr.

Abstract. In this paper, we build and analyze a scheme for variable density flows, able to cope with unstructured non-conforming meshes (*i.e.* with hanging nodes), in $d = 2$ or $d = 3$ space dimensions. The cells are quadrangles ($d = 2$) or hexahedra ($d = 3$), and local refinement is obtained by (possibly successively) dividing some cells in 2^d sub-cells. The space approximation is based on a low-order staggered non-conforming finite element, the so-called Rannacher-Turek element. In the momentum balance equation, a finite element technique is used for the discretization of the diffusion term, where we relax the usual mean value continuity constraint across the mesh faces: at the interface between two refinement levels, average continuity is required only across the coarse face. The convection term is discretized by a finite volume technique, and a careful construction of the momentum fluxes, especially through non-conforming faces, yields a discrete analogue of the kinetic energy identity. On a model problem, namely the steady convection-diffusion equation, we establish a first order error estimate in energy norms. This convergence order is also observed in the numerical experiments for the Navier-Stokes equations, both for incompressible and quasi-incompressible (*i.e.* obeying the asymptotic model for vanishing Mach numbers) flows.

Keywords. Navier-Stokes equations, finite volumes, finite elements, stability, kinetic energy, non-conforming local refinement.

1. Introduction

Let Ω be an open bounded connected subset of $\mathbb{R}^d$, with $d \in \{2, 3\}$, which is supposed to be polygonal if $d = 2$ and polyhedral if $d = 3$, let $T \in \mathbb{R}^+$ and let us consider the following system of equations:

$$\mathcal{C}(\rho, u_i, \boldsymbol{u}) - \mathrm{div}(\boldsymbol{\tau}(\boldsymbol{u}))_i + \partial_i p = 0, \qquad 1 \le i \le d, \qquad \text{on } \Omega \times (0, T), \tag{1.1a}$$

$$\partial_t \rho + \mathrm{div}(\rho \boldsymbol{u}) = 0, \qquad \text{on } \Omega \times (0, T), \tag{1.1b}$$

with $\rho \in \mathbb{R}$, $\boldsymbol{u} = (u_1, \ldots, u_d)^t \in \mathbb{R}^d$ and $p \in \mathbb{R}$ the density, the velocity and the pressure in the flow. The shear stress tensor $\boldsymbol{\tau}$ is given by:

$$\boldsymbol{\tau}(\boldsymbol{u}) = \mu(\boldsymbol{\nabla u} + \boldsymbol{\nabla}^t \boldsymbol{u}) - \frac{2\mu}{3} \mathrm{div}\boldsymbol{u}\, I, \tag{1.2}$$

where μ is a positive parameter, possibly depending on $\boldsymbol{x}$. The operator $\mathcal{C}$ will be referred to in the following as the convection operator and reads:

$$\mathcal{C}(\rho, u_i, \boldsymbol{u}) = \partial_t(\rho u_i) + \mathrm{div}(\rho u_i \boldsymbol{u}), \qquad 1 \le i \le d.$$

The two equations of system (1.1) correspond to the momentum balance and the mass conservation of the fluid, respectively.

Thanks to the mass balance equation, $\mathcal{C}$ may be recast as a transport operator

$$\mathcal{C}(\rho, v, \boldsymbol{u}) = \rho\big(\partial_t v + \boldsymbol{u} \cdot \boldsymbol{\nabla} v\big),$$

for a regular function $v\Omega \times (0,T) \to \mathbb{R}$, and this equivalence between a divergence and transport form allows to show that:

$$\mathcal{C}(\rho, v, \boldsymbol{u})\ \varphi'(v) = \mathcal{C}(\varphi(v)) = \partial_t(\rho\varphi(v)) + \mathrm{div}(\rho\varphi(v)\boldsymbol{u}),$$

for any regular real functions φ. Taking $\varphi(v) = v^2/2$ and $v = u_i$, $1 \leq i \leq d$ yields (at least formally) the kinetic energy identity. We show in [13, Lemma A2] that a discrete analogue of this computation holds for finite volume operators, with a similar interplay between the momentum and mass balances, although with some remainders which turn out to be numerical dissipation terms for convex functions φ. The benefits of such a discrete local kinetic energy identity are two-folds: first, integrating is space and time, it yields stability estimates for incompressible or barotropic flows (see, *e.g.*, [1, 4, 9]); second, it allows to build numerical schemes for compressible flows based on *ad hoc* discretizations of the internal energy balance which preserve the sign of this variable [13]. This latter aspect is particularly interesting for staggered discretizations, where the implementation of the usual techniques relying on (approximate or exact) Riemann solvers is cumbersome. Note also that the conservation of the kinetic energy is often presented as a prerequisite for LES applications [4].

The present work is a continuation of a research program undertaken to develop semi-implicit staggered schemes satisfying a local discrete kinetic energy balance [1, 9, 13, 10]. The convection operator $\mathcal{C}$ is discretized by a finite-volume technique while diffusion terms use, for unstructured meshes, a finite element formulation, in the spirit of the algorithm developed and analyzed for incompressible flows in [23, 24]. For unstructured quadrangular ($d = 2$) or hexahedric ($d = 3$) meshes, we base our space approximation on the Rannacher-Turek element [22]. In the staggered flow context, however, ensuring the above-mentioned required consistency between the mass balance and the momentum convection operator $\mathcal{C}$ is not straightforward, since the mass balance is posed on the primal mesh while the momentum balance equation is posed on the dual mesh. This difficulty is overcome by a construction which derives a secondary mass balance on "dual cells" from the original one; this construction is of algebraic nature, in the sense that it does not require the definition of the dual cells geometry (which, in fact, is never specified). Consequently, the discretization of $\mathcal{C}$ sounds rather abstract, and motivated by stability arguments only. The consistency of this operator was first only suggested by numerical experiments, up to the work in [16] where we show by discrete compactness arguments that, with the stability estimates which are satisfied by the solutions to variable density Navier-Stokes equations, $\mathcal{C}(\rho^{(m)}, u_i^{(m)}, \boldsymbol{u}^{(m)})$ weakly converges to $\mathcal{C}(\bar{\rho}, \bar{u}_i, \bar{\boldsymbol{u}})$, where $\rho^{(m)}$ and $(u_i^{(m)})_{m\in\mathbb{N}}$, $1 \leq i \leq d$, stand for a sequence of discrete solutions which converges, up to the extraction of a subsequence, to $\bar{\rho}$ and $\bar{u}_i$, $1 \leq i \leq d$; we refer to [16] for a more precise formulation of this result. The work presented here builds upon these developments, by pursuing the following goals:

- first, we extend the definition of the discrete velocity convection operator to cope with a class of locally refined non-conforming (*i.e.* featuring hanging nodes) meshes.
- second, we establish an error estimate for the model problem of the convection-diffusion equation which suggests that the discrete convection operator (both on conform or locally refined meshes) is first order accurate for regular solutions. For the diffusion term, we adopt the same finite element approach as for a regular mesh, and the extension to non-conforming meshes is easily obtained in practice by slightly relaxing the weak continuity constraint across a face [3] (mean continuity is required only across the whole face containing the hanging node and not across

each sub-face having this node as vertex). From a theoretical point of view, the error analysis of the resulting approximation turns however to be more technical than in the conforming case.

For numerical tests, the presented scheme is implemented in the open-source software library for fluid applications CALIF^{3}S [5] developed at the French *Institut de Radioprotection et Sûreté Nucléaire* (IRSN), as a building-brick of pressure-correction method (see [6, 25] for the seminal papers and [12] for a review); as a striking outcome of the use of Object Oriented Programming, it is now available for all the software applications, including incompressible, quasi-incompressible (*i.e.* obeying the system of equations obtained at the limit of vanishing MAC numbers [19]) and compressible flows, possibly turbulent or reactive.

This paper is organized as follows. We first describe the space discretization (Section 2) then the proposed convection and diffusion operators for locally refined meshes (Section 3.2). Section 4 is devoted to the error analysis of the scheme on the convection-diffusion model problem, and Section 5 gathers some numerical experiments which comfort this theoretical study.

2. Meshes and discretization spaces

Definition 2.1 (Unrefined mesh)**.** A mesh $\mathcal{M}_0$ is said an unrefined mesh if it is a regular decomposition (in the usual sense of the finite element literature, see *e.g.* [7])) of the domain Ω either in quadrilaterals ($d = 2$) or hexahedra ($d = 3$). Each cell K of $\mathcal{M}_0$ is defined by the image by the standard Q_1 mapping associated with its vertices, denoted by $\mathcal{Q}_K$, of the unit square or cube $(0,1)^d$.

Let us now define a refinement process. In two dimensions, it consists in cutting a cell K in four sub-cells, which are defined as the image by $\mathcal{Q}_K$ of the four sub-squares of the unit square $(\alpha_1/2,\ (\alpha_1+1)/2) \times (\alpha_2/2,\ (\alpha_2+1)/2)$, for $(\alpha_1,\ \alpha_2) \in \{0,1\}^2$. In three dimensions, sub-cells are obtained by applying $\mathcal{Q}_K$ to the eight subset of the unit cube $(\alpha_1/2,\ (\alpha_1+1)/2) \times (\alpha_2/2,\ (\alpha_2+1)/2) \times (\alpha_3/2,\ (\alpha_3+1)/2)$, for $(\alpha_1,\ \alpha_2,\ \alpha_3) \in \{0,1\}^3$. The additional vertices produced by this process lie in the mid-point of a coarse edge in 2D, and at the center of a coarse face in 3D (precisely speaking, at the image by $\mathcal{Q}_K$ of the mass center of the associated face of the reference unit cube). The following lemma is essential for the well-posedness of the refinement process, and is a (not so easy) consequence of the properties of the Q_1 mapping.

Lemma 2.2. *The sub-cells produced by the refinement process are themselves the image of the unit square or cube by the Q_1 mapping associated with their vertices.*

Proof. We give the proof in two dimensions, the extension to $d = 3$ being easy although cumbersome. Let K be a quadrangle of vertices $\boldsymbol{a}_1$, $\boldsymbol{a}_2$, $\boldsymbol{a}_3$ and $\boldsymbol{a}_4$. The cell K is thus defined by:

$$K = \Big\{ \sum_{i=1}^{4} \varphi_i(\hat{\boldsymbol{x}})\ \boldsymbol{a}_i,\ \hat{\boldsymbol{x}} \in (0,1)^2 \Big\},$$

with $\varphi_1(\hat{\boldsymbol{x}}) = (1-\hat{x}_1)\,(1-\hat{x}_2)$, $\varphi_2(\hat{\boldsymbol{x}}) = \hat{x}_1\,(1-\hat{x}_2)$, $\varphi_3(\hat{\boldsymbol{x}}) = \hat{x}_1\,\hat{x}_2$ and $\varphi_4(\hat{\boldsymbol{x}}) = (1-\hat{x}_1)\,\hat{x}_2$. A fundamental property of the Q_1 mapping is that it may be obtained by 2 (in fact d) successive interpolations, performed in any order. Indeed, let us denote by $\mathcal{I}(\boldsymbol{a}, \boldsymbol{b}, s)$ the following interpolated point between $\boldsymbol{a}$ and $\boldsymbol{b}$:

$$\mathcal{I}(\boldsymbol{a}, \boldsymbol{b}, s) = (1-s)\,\boldsymbol{a} + s\boldsymbol{b}.$$

Then, by the definition of φ, we get:

$$K = \big\{ \mathcal{I}\big(\mathcal{I}(\boldsymbol{a}_1, \boldsymbol{a}_4, \hat{x}_2),\ \mathcal{I}(\boldsymbol{a}_2, \boldsymbol{a}_3, \hat{x}_2),\ \hat{x}_1\big),\ \hat{\boldsymbol{x}} \in (0,1)^2 \big\}.$$

In addition, we may check that a first property of the interpolation operator $\mathcal{I}$ is that, for any vector $\hat{\boldsymbol{x}}$ of $\mathbb{R}^2$:

$$\mathcal{I}\big(\mathcal{I}(\boldsymbol{a}_1, \boldsymbol{a}_4, \hat{x}_2),\ \mathcal{I}(\boldsymbol{a}_2, \boldsymbol{a}_3, \hat{x}_2),\ \hat{x}_1\big) = \mathcal{I}\big(\mathcal{I}(\boldsymbol{a}_1, \boldsymbol{a}_2, \hat{x}_1),\ \mathcal{I}(\boldsymbol{a}_4, \boldsymbol{a}_3, \hat{x}_1),\ \hat{x}_2\big).$$

Let $\boldsymbol{a}_{1,4}$ be defined by $\boldsymbol{a}_{1,4} = (\boldsymbol{a}_1 + \boldsymbol{a}_4)/2$. Then, it is easy to see that $\mathcal{I}$ also satisfies:

$$\big\{\mathcal{I}(\boldsymbol{a}_1, \boldsymbol{a}_4, s),\ s \in (0, 1/2)\big\} = \big\{\mathcal{I}(\boldsymbol{a}_1, \boldsymbol{a}_{1,4}, s),\ s \in (0,1)\big\}.$$

We a similar definition for $\boldsymbol{a}_{1,3}$, we get for the first sub-cell of K, let us say K_1:

$$\begin{aligned} K_1 &= \big\{\mathcal{I}\Big(\mathcal{I}(\boldsymbol{a}_1, \boldsymbol{a}_4, \hat{x}_2),\ \mathcal{I}(\boldsymbol{a}_2, \boldsymbol{a}_3, \hat{x}_2),\ \hat{x}_1\Big),\ \hat{\boldsymbol{x}} \in (0, \frac{1}{2})^2\big\} \\ &= \big\{\mathcal{I}\Big(\mathcal{I}(\boldsymbol{a}_1, \boldsymbol{a}_{1,4}, \xi),\ \mathcal{I}(\boldsymbol{a}_2, \boldsymbol{a}_{2,3}, \xi),\ \hat{x}_1\Big),\ \hat{x}_1 \in (0, \frac{1}{2}),\ \xi \in (0,1)\big\}. \end{aligned}$$

We now permute the interpolations to obtain:

$$K_1 = \big\{\mathcal{I}\Big(\mathcal{I}(\boldsymbol{a}_1, \boldsymbol{a}_2, \hat{x}_1),\ \mathcal{I}(\boldsymbol{a}_{1,4}, \boldsymbol{a}_{2,3}, \hat{x}_1),\ \xi\Big),\ \hat{x}_1 \in (0, \frac{1}{2}),\ \xi \in (0,1)\big\}.$$

Finally, with $\boldsymbol{a}_{1,2} = (\boldsymbol{a}_1 + \boldsymbol{a}_2)/2$ and $\boldsymbol{a}_{1,2,3,4} = (\boldsymbol{a}_1 + \boldsymbol{a}_2 + \boldsymbol{a}_3 + \boldsymbol{a}_4)/4$, we get:

$$K_1 = \big\{\mathcal{I}\Big(\mathcal{I}(\boldsymbol{a}_1, \boldsymbol{a}_{1,2}, \eta),\ \mathcal{I}(\boldsymbol{a}_{1,4}, \boldsymbol{a}_{1,2,3,4}, \eta),\ \xi\Big),\ (\eta, \xi) \in (0,1)^2\big\}.$$

This means that K_1 may be obtained from the unit square by the Q_1 mapping associated with the vertices $\boldsymbol{a}_1$, $\boldsymbol{a}_{1,2}$, $\boldsymbol{a}_{1,2,3,4}$ and $\boldsymbol{a}_{1,4}$, which is the result we are searching for. The same conclusion may be obtained for the other sub-cells of K, by simple change of axes for the unit square. In three dimensions, the proof follows similar lines, but the interpolation operator $\mathcal{I}$ must be applied three times (along each of the coordinates) instead of twice. ■

We are now in position to define a locally refined mesh.

Definition 2.3 (Refined mesh)**.** A locally refined mesh is obtained from an unrefined one by recursively splitting some cells by the above defined refinement process, in such a way that the number of hanging nodes per face is at most one (which means that the difference of level of refinement between two adjacent cells is at most one).

Examples of locally refined meshes are given on Figure 1.

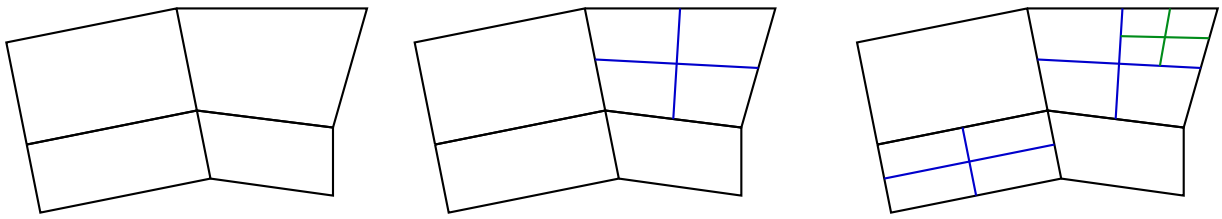

(a) (b) (c)

Figure 1. An example of admissible mesh refinement – (a): conforming mesh. (b): refined mesh obtained by cutting in four some initial cells (process often called "first level refinement"). (c): refined mesh obtained by cutting in four some initial cells and some refined cells ("second level refinement"). The edges in blue and green are created by the first end second refinement level, respectively.

We denote by $\mathcal{M}$ the obtained mesh by such a refinement process, and by $\mathcal{E}(K)$ the set of the faces of an element $K \in \mathcal{M}$. We exclude the presence of a node in the interior of a face, *i.e.* we split an initial face in 2^{d-1} faces if one of the cells adjacent to the face is split. The number of faces, $N_K^{\mathcal{E}}$, of a cell K thus ranges between $2d$ and $2^d d$. Let $\mathcal{E} = \cup_{K \in \mathcal{M}} \mathcal{E}(K)$, $\mathcal{E}_{\text{ext}} = \{\sigma \in \mathcal{E}, \sigma \subset \partial\Omega\}$ and $\mathcal{E}_{\text{int}} = \mathcal{E} \setminus \mathcal{E}_{\text{ext}}$.

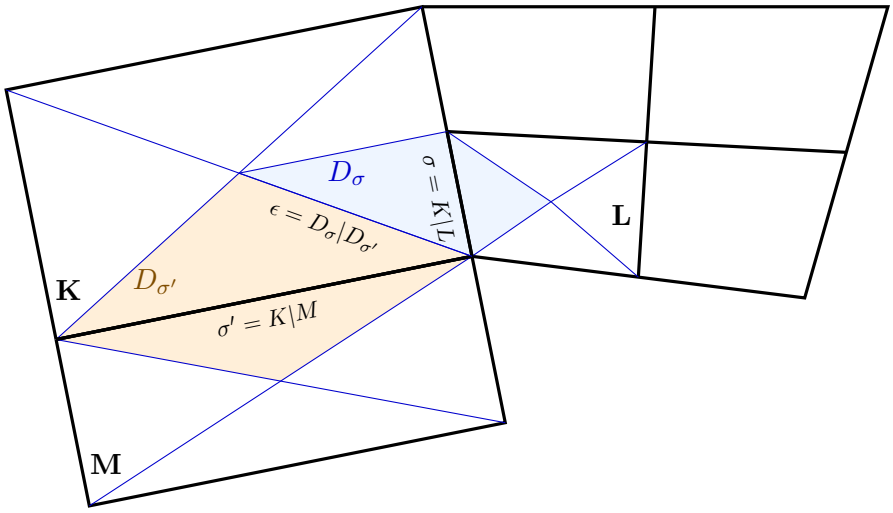

FIGURE 2. Notations for control volumes and diamond cells.

A face $\sigma \in \mathcal{E}_{\rm int}$ separating the cells K and L is denoted by $K|L$. Hereafter, $|\cdot|$ stands for the d- or $(d-1)$-dimensional measure of a subset of $\mathbb{R}^d$ or $\mathbb{R}^{d-1}$ respectively.

For $\sigma \in \mathcal{E}(K)$, $\boldsymbol{n}_{K,\sigma}$ stands for a unit normal vector to σ outward K. In two dimensions and for plane faces in three dimensions, its definition is clear. For non-plane faces, many definitions are possible; here, we split the face in four 2-dimensional simplices the boundary of which joins the center of the face (with the same definition as before, namely the image by $\mathcal{Q}_K$ of the mass center of the associated face of the unit cube) and two vertices of the face, and use for $\boldsymbol{n}_{K,\sigma}$ the average of the unit normal vectors of these four simplices, weighted by their area.

We define a dual mesh associated with the faces $\mathcal{E}$ as follows. When $K \in \mathcal{M}$ is a rectangle or a cuboid, for $\sigma \in \mathcal{E}(K)$, we define the half-diamond cell $D_{K,\sigma}$ as the cone with basis σ and with vertex the mass center of K (see Figure 2). We thus obtain a partition of K in $N_K^{\mathcal{E}}$ sub-volumes, each sub-volume having a measure $|D_{K,\sigma}|$ equal to $|K|/(2d)$, when σ has not been split, or $|K|/(2^d d)$ otherwise. We extend this definition to general quadrangles and hexahedra, by supposing that we have built a partition with the same connectivities and the same ratio between the volumes of the half-diamonds and of the cell. For $\sigma \in \mathcal{E}_{\rm int}$, $\sigma = K|L$, we now define the dual (or diamond) cell D_σ associated with σ by $D_\sigma = D_{K,\sigma} \cup D_{L,\sigma}$. For $\sigma \in \mathcal{E}(K) \cap \mathcal{E}_{\rm ext}$, we define $D_\sigma = D_{K,\sigma}$. We denote by $\tilde{\mathcal{E}}(D_\sigma)$ the set of faces of D_σ, and by $\epsilon = D_\sigma|D_{\sigma'}$ the face separating two dual cells D_σ and $D_{\sigma'}$ (see Figure 2).

The space discretization is staggered in the sense that the pressure and the velocity unknowns are discretized as piecewise constant functions respectively on the primal and dual mesh. In addition, in order for the algorithm to be further suitable for more general models including the density as unknown (*e.g.* the asymptotic model for anisothermal low Mach number flows, see Section 5.3), we suppose that ρ is approximated by a discrete function which is also piecewise constant on the primal mesh. Hence, the degrees of freedom for the pressure and the density are associated with the cells of the primal mesh: $\{p_K,\ K \in \mathcal{M}\}$ and $\{\rho_K,\ K \in \mathcal{M}\}$ while a discrete velocity field is associated with degrees of freedom localized at the cells of the dual mesh: $\{\boldsymbol{u}_\sigma,\ \sigma \in \mathcal{E}\}$.

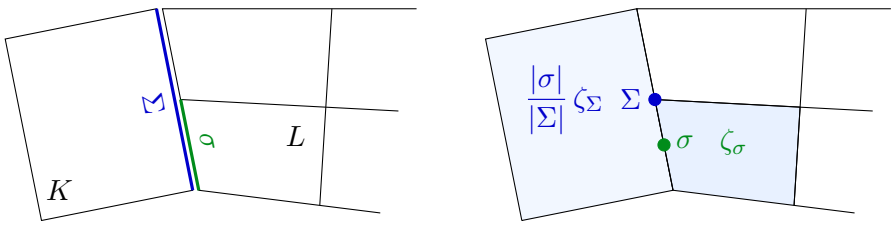

Figure 3. Piecewise definition of ζ_σ.

3. The discrete diffusion and convection operators

The purpose of this section is to define the discrete diffusion and convection operators for the cells adjacent to faces featuring a hanging node.

3.1. The diffusion operator

The discretization of the diffusion term $-(\mathrm{div}\boldsymbol{\tau}(\boldsymbol{u}))$ relies on the so-called "rotated bi-linear element" introduced by Rannacher and Turek [22]. The reference element $\widehat{K}$ is the unit d-cube $(0,1)^d$, and the discrete functional space is:

$$\widetilde{Q}_1(\widehat{K}) = \mathrm{span}\left\{1,\ (\boldsymbol{x}_i)_{i=1,\dots,d},\ (\boldsymbol{x}_i^2 - \boldsymbol{x}_{i+1}^2)_{i=1,\dots,d-1}\right\}. \tag{3.1}$$

When no vertex of the face σ is a hanging node, we impose the jump of a discrete function through the face to have a zero mean value. When one vertex is a hanging node, we only impose to zero the integral of the jump through the initial coarse face containing σ. Hence, the set $\{\zeta_\sigma,\ \sigma\in\mathcal{E}\}$ of nodal functions associated with the Rannacher-Turek element is defined as follows.

Let $K\in\mathcal{M}$ and σ be a face of K. If σ is a whole side of K, the standard definition applies:

$$\begin{aligned} &(i) \qquad \zeta_\sigma|_K = \zeta_{\widehat{\sigma}}\circ\mathcal{Q}_K^{-1} \text{ where } \zeta_{\widehat{\sigma}} \text{ is some function of } \widetilde{Q}_1(\widehat{K}),\\ &(ii) \qquad \frac{1}{|\sigma|}\int_\sigma \zeta_\sigma = 1 \text{ and, for all other sides } \Sigma' \text{ of } K,\ \int_{\Sigma'}\zeta_\sigma = 0. \end{aligned} \tag{3.2}$$

Let us now suppose that σ is only a subset of a side of K, which we denote by Σ (which occurs when σ separates K form a cell which refinement level is equal to the refinement level of K plus 1, see Figure 3). Let ζ_Σ be the Rannacher-Turek usual shape function associated with Σ (*i.e.* the function satisfying the above definition (3.2), replacing σ by Σ). Then, we define ζ_σ on K by:

$$\zeta_\sigma(\boldsymbol{x}) = \frac{|\sigma|}{|\Sigma|}\zeta_\Sigma(\boldsymbol{x}).$$

Finally, of course, the nodal functions are local, in the sense that, for $\sigma\in\mathcal{E}$, the support of ζ_σ is reduced to the (one or two) cells adjacent to σ.

We are now in position to apply a Galerkin technique, which yields, for the discretization of the i^{th} component of the diffusion term:

$$-(\mathrm{div}\boldsymbol{\tau}(\boldsymbol{u}))_{\sigma,i} = \frac{1}{|D_\sigma|}\sum_{K\in\mathcal{M}}\int_K \sum_{\sigma'\in\mathcal{E}(K)}\sum_{j=1}^{d}\boldsymbol{u}_{\sigma',j}\ \boldsymbol{\tau}\big(\zeta_{\sigma'}(\boldsymbol{x})\,\boldsymbol{e}^{(j)}\big) : \boldsymbol{\nabla}\big(\zeta_\sigma(\boldsymbol{x})\,\boldsymbol{e}^{(i)}\big)\,\mathrm{d}\boldsymbol{x},$$

where, for $1\le j\le d$, $\boldsymbol{e}^{(j)}$ stands for the j^{th} vector of the canonical basis of $\mathbb{R}^d$.

3.2. **The discrete momentum convection operator**

We now turn to the approximation of the convection operator $\mathcal{C} = \partial_t(\rho u) + \mathrm{div}(u\boldsymbol{q})$, which appears in the momentum balance equation (1.1a) with ρ the density, u a component of the velocity, and $\boldsymbol{q} = \rho\boldsymbol{u}$ the momentum field. This approximation is of finite volume type, with a discretization based on the diamond cells, and takes the following general form, for $\sigma \in \mathcal{E}_{\rm int}$:

$$\mathcal{C}_\sigma^n = \frac{1}{\delta t}(\rho_\sigma^n u_\sigma^n - \rho_\sigma^{n-1} u_\sigma^{n-1}) + \frac{1}{|D_\sigma|} \sum_{\epsilon \in \tilde{\mathcal{E}}(D_\sigma)} F_{\sigma,\epsilon}^n \, u_\epsilon^n.$$

The quantities ρ_σ^n and ρ_σ^{n-1} are approximations of the density on the dual cell D_σ at time t_n and t_{n-1} respectively, and the quantities $F_{\sigma,\epsilon}^n$ are mass fluxes across the faces of the dual cells. These quantities are built so that a finite volume discretization of the mass balance holds over the internal dual cells:

$$\frac{1}{\delta t}\,(\rho_\sigma^n - \rho_\sigma^{n-1}) + \frac{1}{|D_\sigma|} \sum_{\epsilon \in \tilde{\mathcal{E}}(D_\sigma)} F_{\sigma,\epsilon}^n = 0, \qquad \sigma \in \mathcal{E}_{\rm int}. \tag{3.3}$$

This is crucial in order to reproduce, at the discrete level, an analogue of the relation $\mathcal{C}\ u = \frac{1}{2}\partial_t(\rho u^2) + \frac{1}{2}\mathrm{div}(u^2\boldsymbol{q})$, which a central arguments of stability estimates. Relation (3.3) must be deduced from the mass balance solved by the scheme, which is supposed to take the following form:

$$\frac{1}{\delta t}\,(\rho_K^n - \rho_K^{n-1}) + \frac{1}{|K|} \sum_{\epsilon \in \mathcal{E}(K)} F_{K,\sigma}^n = 0, \qquad K \in \mathcal{M}, \tag{3.4}$$

with $F_{K,\sigma}^n$ the mass flux through σ outward K at time t_n, the expression of which does not need to be specified here.

Let us now give the detailed construction of the dual densities and mass fluxes that ensures (3.3). For $\sigma \in \mathcal{E}_{\rm int}$ such that $\sigma = K|L$, the approximate densities on the dual cell D_σ are given by the following weighted average:

$$|D_\sigma|\ \rho_\sigma^k = \xi_K^\sigma |K|\ \rho_K^k + \xi_L^\sigma |L|\ \rho_L^k, \qquad \text{for } k = n-1 \text{ and } k = n, \tag{3.5}$$

where

$$\xi_K^\sigma = \frac{|D_{K,\sigma}|}{|K|}, \qquad K \in \mathcal{M},\ \sigma \in \mathcal{E}(K). \tag{3.6}$$

The set of dual fluxes $F_{\sigma,\epsilon}^n$ with ϵ included in the primal cell K, is computed by solving a linear system which right-hand side is a linear combination of the primal fluxes $(F_{K,\sigma}^n)_{\sigma\in\mathcal{E}(K)}$, appearing in the discrete mass balance (3.4). More precisely, we have the following definition for the dual fluxes, in which we omit for short the time dependence (*i.e.* the superscript n).

Definition 3.1 (Definition of the dual fluxes from the primal ones)**.** The fluxes through the faces of the dual mesh are defined so as to satisfy the following three constraints:

- *(H1)* – For all primal cell K in $\mathcal{M}$, the set $(F_{\sigma,\epsilon})_{\epsilon\subset K}$ of dual fluxes through faces included in K satisfies the following linear system:

$$F_{K,\sigma} + \sum_{\epsilon \in \tilde{\mathcal{E}}(D_\sigma),\ \epsilon \subset K} F_{\sigma,\epsilon} = \xi_K^\sigma \sum_{\sigma' \in \mathcal{E}(K)} F_{K,\sigma'}, \qquad \forall \sigma \in \mathcal{E}(K). \tag{3.7}$$

- *(H2)* – The dual fluxes are conservative: $F_{\sigma,\epsilon} = -F_{\sigma',\epsilon}$ for all $\epsilon = D_\sigma | D'_\sigma$.

- *(H3)* – The dual fluxes are bounded with respect to the primal ones $(F_{K,\sigma})_{\sigma\in\mathcal{E}(K)}$:

$$|F_{\sigma,\epsilon}| \le\ C \max\left\{|F_{K,\sigma}|,\ \sigma \in \mathcal{E}(K)\right\}, \qquad K \in \mathcal{M},\ \sigma \in \mathcal{E}(K),\ \epsilon \in \tilde{\mathcal{E}}(D_\sigma),\ \epsilon \subset K.$$

Appendix A provides the detailed construction of the dual fluxes (*i.e.* the way to find a solution to (3.7) satisfying the other two constraints). Owing to these definitions of the dual densities and mass fluxes, the mass balance on the dual cells (3.3) is an easy consequence of the mass balance on the cells of the primal mesh (3.4) [1].

To make the description of the operator complete, it remains to define the velocity interpolates $\boldsymbol{u}_\epsilon^n$ at the internal dual faces. We chose a centered approximation:

$$\boldsymbol{u}_\epsilon^n = \frac{\boldsymbol{u}_\sigma^n + \boldsymbol{u}_{\sigma'}^n}{2}, \qquad \text{for } \epsilon = D_\sigma | D'_\sigma.$$

4. Error analysis for the advection-diffusion equation

For the sake of simplicity, we propose to perform an error analysis of the scheme on the simplified model of the advection-diffusion equation. This scalar equation can be seen as a model problem for the prediction step of the method (for one component of the velocity), where the known density is assumed to be constant and the pressure gradient and the advective velocity are known given functions from the previous time step. Since the density is considered constant, the mass balance $\partial_t \rho + \mathrm{div}(\rho \boldsymbol{w}) = 0$ boils down to $\mathrm{div}\boldsymbol{w} = 0$, which is supposed here; this relation plays, for the stability of the model problem under consideration, the same role as the kinetic energy identity in Navier-Stokes equations. We assume in addition that $\boldsymbol{w}$ is a regular function, namely $\boldsymbol{w} \in \mathrm{C}^1(\bar{\Omega})^d$, and vanishes at the boundary $\partial\Omega$ of the computational domain. The problem we consider thus consists in finding a function u such that:

$$u + \mathrm{div}(u\boldsymbol{w}) - \boldsymbol{\Delta} u = f, \qquad \text{on } \Omega, \tag{4.1a}$$

$$u = 0, \qquad \text{on } \partial\Omega, \tag{4.1b}$$

where $f \in \mathrm{L}^2(\Omega)$. In order to write a weak formulation of (4.1), let us define the following forms corresponding respectively to the diffusion and convection terms:

$$a(u,v) = \int_\Omega \boldsymbol{\nabla} u \cdot \boldsymbol{\nabla} v, \quad b(\boldsymbol{w},u,v) = \int_\Omega \mathrm{div}(u\boldsymbol{w}) v, \quad u,v \in \mathrm{H}_0^1(\Omega).$$

We also introduce the inner product of $\mathrm{L}^2(\Omega)$ denoted $(.,.)$, and we are now in position to state the weak formulation of problem (4.1).

Definition 4.1. A weak solution of the advection-diffusion problem (4.1) is a function $u \in \mathrm{H}_0^1(\Omega)$ such that:

$$(u,v) + b(\boldsymbol{w},u,v) + a(u,v) = (f,v), \qquad \forall v \in \mathrm{H}_0^1(\Omega). \tag{4.2}$$

It is well known that, by the Lax-Milgram theorem, there exists a unique solution to (4.2).

4.1. Regularity of the mesh and approximation space

In addition to the definition of the mesh given in Section 2, we suppose that any quadrilaterals ($d = 2$) or hexahedra ($d = 3$) of the mesh are convex, which implies that their faces are hyperplanes of $\mathbb{R}^d$. For $K \in \mathcal{M}$, we denote by h_K the diameter of K. Similarly, we denote by h_σ the diameter of an edge $\sigma \in \mathcal{E}$. The size of the discretization is defined as usual by:

$$h = \max\{h_K, K \in \mathcal{M}\}.$$

For the consistency of the Rannacher-Turek finite element approximation of the diffusion term, we need a measure of the difference between the cells of $\mathcal{M}$ and parallelograms ($d = 2$) or parallelepipeds ($d = 3$), as defined in [22]. For $K \in \mathcal{M}$, we denote by $\bar{\alpha}_K$ the maximum of the angles between the normal vectors of opposite faces, choosing for the latter the orientation which maximizes the angle,

and set $\alpha_K = \pi - \bar{\alpha}_K$ (so $\alpha_K = 0$ if K is a parallelogram or a parallelepiped, and $\alpha_K > 0$ otherwise). Then we define α_h as:

$$\alpha_h = \max\{\alpha_K,\ K \in \mathcal{M}\}. \tag{4.3}$$

For $K \in \mathcal{M}$, let $\{\boldsymbol{a}_{i,K},\ i = 1,..,2^d\}$ denote the vertices of K. Let $\boldsymbol{a}_{i,K}$ be one of these vertices and let $S_{i,K}$ be the simplex whose vertices are $\boldsymbol{a}_{i,K}$ and the d adjacent vertices to $\boldsymbol{a}_{i,K}$. We denote by $r_{i,K}$ the diameter of the largest ball included in $S_{i,K}$ and by r_K the real number given by $r_K = \min\{r_{i,K},\ i = 1,..,2^d\}$. We define the real number θ_h by:

$$\theta_h = \max\left\{\frac{h_K}{r_K},\ K \in \mathcal{M}\right\}. \tag{4.4}$$

In accordance with the velocity discretization described in Section 3, a discrete function v is associated with degrees of freedom $\{v_\sigma,\ \sigma \in \mathcal{E}_{\rm int}\}$ located at the internal faces, the values associated with the boundary faces $\mathcal{E} \in \mathcal{E}_{\rm ext}$ being set to zero, consistently with the boundary conditions (4.1b). For $K \in \mathcal{M}$, the restriction of a discrete function v to K belongs to the local Rannacher-Turek space: $v|_K = \widehat{v} \circ \mathcal{Q}_K^{-1}$ where $\widehat{v} \in \widetilde{Q}_1(\widehat{K})$ (see (3.1)). The last step to obtain a definition of the discrete approximation space is to state the continuity constraints satisfied by the discrete functions at the faces. Once again, when no vertex of the face is a hanging node, this issue is clear: as usual for the Rannacher-Turek element, we impose the jump through the face to have a zero mean value. Otherwise, we only impose to zero the integral of the jump through the initial coarse face. Hence the approximation space is given by

$$V_h = \big\{v(\boldsymbol{x}) = \sum_{\sigma \in \mathcal{E}_{\rm int}} v_\sigma\ \zeta_\sigma(\boldsymbol{x}), \quad (v_\sigma)_{\sigma \in \mathcal{E}_{\rm int}} \subset \mathbb{R}\big\}, \tag{4.5}$$

where the shape functions ζ_σ are defined in Section 3.1.

With the continuity requirements described above, the functions of V_h are discontinuous across each edge; the discretization is thus non-conforming in the sense that $V_h \not\subset \mathrm{H}^1_0(\Omega)$. Therefore we define the "broken" gradient $\boldsymbol{\nabla}_h v$ on V_h as the function of $\mathrm{L}^2(\Omega)^d$ which is equal to $\boldsymbol{\nabla} v|_K$ for all $K \in \mathcal{M}$. The corresponding broken Sobolev H^1 semi-norm is defined for $v \in V_h$ by:

$$\|v\|^2_{h,\mathrm{b}} = \int_\Omega |\boldsymbol{\nabla}_h v|^2 = \sum_{K \in \mathcal{M}} \int_K |\boldsymbol{\nabla} v|^2.$$

Thanks to the homogeneous Dirichlet boundary conditions, this defines a norm on V_h which is known to control the L^2-norm by a Poincaré inequality:

$$\|v\|_{\mathrm{L}^2(\Omega)} \le \mathrm{diam}(\Omega)\ \|v\|_{h,\mathrm{b}}, \qquad \forall v \in V_h. \tag{4.6}$$

4.2. **The staggered scheme for the advection-diffusion equation**

Let us now adapt to the advection-diffusion problem the first step of the staggered scheme proposed in Section 3. For this purpose, we assume that the divergence of the velocity field $\boldsymbol{w}$ is discretized on the cells of the primal mesh by

$$\mathrm{div}(\boldsymbol{w})|_K \approx \frac{1}{|K|} \sum_{\sigma \in \mathcal{E}(K)} F_{K,\sigma}(\boldsymbol{w}), \quad \text{with} \quad F_{K,\sigma}(\boldsymbol{w}) = \int_\sigma \boldsymbol{w} \cdot n_{K,\sigma}\, \mathrm{d}\gamma, \tag{4.7}$$

and we define the dual fluxes $F_{\sigma,\epsilon}(\boldsymbol{w})$ from the primal ones following exactly the procedure described in Section 3.2. Adapting the staggered scheme to the advection-diffusion problem thus consists in finding a discrete function $u_h \in V_h$ such that:

$$(u_h, v)_h + b_h(\boldsymbol{w}, u_h, v) + a_h(u_h, v) = (f, v), \qquad \text{for all } v \in V_h, \tag{4.8}$$

where, for any $u,\ v \in V_h$,

$$(u,v)_h = \sum_{\sigma\in\mathcal{E}} |D_\sigma| u_\sigma v_\sigma, \tag{4.9}$$

$$b_h(\boldsymbol{w},u,v) = \sum_{\sigma\in\mathcal{E}} v_\sigma \sum_{\epsilon\in\tilde{\mathcal{E}}(D_\sigma)} F_{\sigma,\epsilon}(\boldsymbol{w})\, u_\epsilon, \tag{4.10}$$

$$a_h(u,v) = \int_\Omega \boldsymbol{\nabla}_h u \cdot \boldsymbol{\nabla}_h v. \tag{4.11}$$

4.3. **Stability properties of the scheme**

One first important property of the scheme follows from the particular construction of the discrete convection term $b_h(\boldsymbol{w},u,v)$. Indeed, since $\boldsymbol{w}$ is divergence-free, one has

$$\sum_{\sigma\in\mathcal{E}(K)} F_{K,\sigma}(\boldsymbol{w}) = 0,$$

which, by construction, implies a similar discrete divergence-free property on the cells of the dual mesh:

$$\sum_{\epsilon\in\tilde{\mathcal{E}}(D_\sigma)} F_{\sigma,\epsilon}(\boldsymbol{w}) = 0, \qquad \forall\sigma\in\mathcal{E}_{\rm int}. \tag{4.12}$$

This is crucial in order to reproduce, at the discrete level, the derivation of a stability estimate for the scheme, analogous to the kinetic energy balance equation in the context of the full Navier-Stokes equations. Indeed, by a computation which may be found in [1], Equation (4.12) yields:

$$b_h(\boldsymbol{w},v,v) = 0, \qquad \forall v\in V_h. \tag{4.13}$$

Remark 4.2. At first glance, this relation is the usual well known antisymmetry of the centered convection operator with a divergence free advection field; note however that the scheme is posed on a dual mesh, which, if we restrict the set of dual cells to those associated with the internal faces, does not cover Ω, and that no balance equation is written on the remainder of the domain (*i.e.* the half-diamond-shaped volumes associated with the external faces). This necessitates a slight adaptation of the usual proof, which is performed in [1].

A first consequence of this antisymmetry property is the existence of a unique solution to the scheme (4.8). Let $\mathcal{A}_h$ be the following form defined on the finite dimensional space $V_h \times V_h$ by

$$\mathcal{A}_h(u,v) = (u,v)_h + b_h(\boldsymbol{w},u,v) + a_h(u,v), \qquad u,v\in V_h.$$

The mapping Φ from V_h to V_h' which maps an element u to the form $\Phi(u) := \mathcal{A}_h(u,.)$ is clearly linear and satisfies $(\Phi(u)=0 \Rightarrow u=0)$ since $\mathcal{A}_h(u,u) = (u,u)_h + \|u\|^2_{h,\rm b}$ for all $u\in V_h$ by (4.13). Hence, Φ is a one-to-one linear mapping which, in a finite dimensional context, is equivalent to the existence of a unique solution $u_h\in V_h$ which satisfies $\Phi(u_h) = f$ *i.e.* $\mathcal{A}_h(u,v) = (f,v)$ for all $v\in V_h$.

A second straightforward consequence is a stability estimate on the solution u_h. Taking u_h as a test function in (4.8) and using again (4.13), one gets $(u_h,u_h)_h + \|u_h\|^2_{h,\rm b} = (f,u_h)$. Applying Young's inequality in the right hand side term and recalling the Poincaré inequality (4.6), we obtain the stability estimate

$$2\,(u_h,u_h)_h + \|u_h\|^2_{h,\rm b} \le \mathrm{diam}(\Omega)^2\ \|f\|^2_{\mathrm{L}^2(\Omega)}. \tag{4.14}$$

4.4. **Error estimate**

We may now state the main result of this section, which is an error estimate for the scheme (4.8).

Theorem 4.3. *Let $\theta_0 > 0$ and let $\mathcal{M}$ be a locally refined mesh of the computational domain Ω (in the sense of Definition 2.3) such that $\theta_h \leq \theta_0$, with θ_h defined by* (4.4)*. Let $u_h \in V_h$ be the solution to the scheme* (4.8)*. We assume that the solution u of the continuous problem* (4.2) *belongs to* $\mathrm{H}^1_0(\Omega) \cap \mathrm{H}^2(\Omega)$*. Then u_h satisfies:*

$$\|u_h - u\|_{h,\mathrm{b}} \leq C\,(h + \alpha_h)\ \|u\|_{\mathrm{H}^2(\Omega)},$$

where C only depends on $\boldsymbol{w}$, Ω and θ_0.

Remark 4.4 (A particular construction of a regular sequence of discretizations)**.** For $d = 2$, a sequence of discretizations satisfying $h \to 0$ and $\alpha_h \to 0$ is obtained by successively dividing each quadrangle in four sub-quadrangles, splitting it along the lines joining the mid-points of opposite faces. Unfortunately, the extension of this construction to the three-dimensional case is not straightforward, since this subdivision process may generate non-plane faces (see Appendix B).

Remark 4.5. Theorem 4.3 shows that the accuracy of the scheme for the energy norm $\|.\|_{h,\mathrm{b}}$ is the same as that of the usual Rannacher-Turek approximation of the Stokes problem on non-refined meshes [22]. In particular, there is no loss in the convergence rate due to the non-conforming local refinement or the particular discretization of the convection term.

4.4.1. *Preliminary lemmas*

We begin with stating some technical lemmas, which will be useful in the proof of Theorem 4.3. We first introduce the following discrete H^1-norm on the space V_h:

$$\|v\|^2_{h,\mathrm{fv}} = \sum_{K\in\mathcal{M}} h_K^{d-2} \sum_{\sigma,\sigma'\in\mathcal{E}(K)} |v_\sigma - v_{\sigma'}|^2, \tag{4.15}$$

which, by an easy computation, may be shown to be equivalent, over a regular sequence of discretizations such that $\max_h \theta_h \leq \theta_0$ for some $\theta_0 > 0$, to the usual finite volume H^1-norm. Lemma 4.6 shows that this H^1-norm is controlled by the broken-Sobolev H^1-norm.

Lemma 4.6. *Let $\theta_0 > 0$ and let $\mathcal{M}$ be a locally refined mesh of the computational domain Ω such that $\theta_h \leq \theta_0$, with θ_h defined by* (4.4)*. Then, there exists C only depending on θ_0 such that:*

$$\|v\|_{h,\mathrm{fv}} \leq C\ \|v\|_{h,\mathrm{b}}, \quad \forall v \in V_h.$$

Proof. For $K \in \mathcal{M}$, let $\widehat{v}$ be the function defined over $\widehat{K}$ by $\widehat{v}(\widehat{\boldsymbol{x}}) = v(\boldsymbol{x})$, where $\boldsymbol{x} \in K$ stands for the image of $\widehat{\boldsymbol{x}}$ by the Q_1 mapping $\mathcal{Q}_K$. By definition of the discretization space, we have $\widehat{v} \in \widetilde{Q}_1(\widehat{K})$. Now, since there exists only a bounded number of possible configurations for K (depending on the fact that its sides are split in 2^{d-1} faces or not), a finite dimensional argument for norms acting on $\widetilde{Q}_1(\widehat{K})$ shows that there exists a constant C such that:

$$\sum_{\sigma,\sigma'\in\mathcal{E}(K)} |v_\sigma - v_{\sigma'}|^2 \leq C\ \int_{\widehat{K}} |\boldsymbol{\nabla}\widehat{v}|^2.$$

We conclude the proof by invoking standard properties of the Q_1 mapping which enable to write:

$$\int_{\widehat{K}} |\boldsymbol{\nabla}\widehat{v}|^2 \leq C(\theta_0)\frac{h_K^2}{|K|}\int_K |\boldsymbol{\nabla}v|^2 \leq C'(\theta_0)h_K^{2-d}\int_K |\boldsymbol{\nabla}v|^2.$$

■

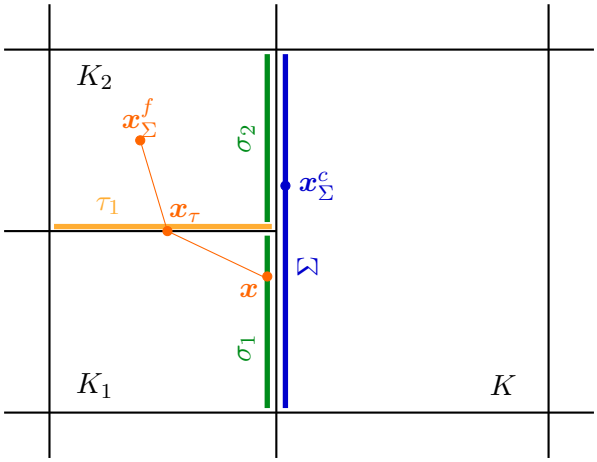

FIGURE 4. Notations for the proof of Lemma 4.8.

The following lemma compares piecewise constant approximates of a discrete function with the function itself. It is an easy consequence of the previous one.

Lemma 4.7. *Let $\theta_0 > 0$ and let $\mathcal{M}$ be a locally refined mesh of the computational domain Ω such that $\theta_h \leq \theta_0$, with θ_h defined by (4.4). For $v \in V_h$, let $v_{\rm c}$ stand for the piecewise constant function over each diamond cell D_σ and equal to v_σ. Then, there exists C, only depending on θ_0, such that:*

$$\|v - v_{\rm c}\|_{{\rm L}^2(\Omega)} \leq C\, h\, \|v\|_{h,{\rm b}}.$$

Let now $v_{\rm m}$ be defined as a piecewise constant function over the primal mesh, the value over a cell K being a convex combination of $(v_\sigma)_{\sigma\in\mathcal{E}(K)}$. Then, once again, there exists C, only depending on θ_0, such that:

$$\|v - v_{\rm m}\|_{{\rm L}^2(\Omega)} \leq C\, h\, \|v\|_{h,{\rm b}}.$$

The following lemma is the analogue, for the Rannacher-Turek element and a locally refined mesh, of a well known result for the Crouzeix-Raviart element and regular meshes. For technical reasons, its proof is however more intricate than in the case of conforming meshes.

Lemma 4.8. *Let $\theta_0 > 0$ and let $\mathcal{M}$ be a locally refined mesh of the computational domain Ω such that $\theta_h \leq \theta_0$, with θ_h defined by (4.4). Let $v \in V_h$. For $\sigma \in \mathcal{E}_{\rm int}$, let $[v]_\sigma$ denote the jump of v across σ (the orientation of which we do not need to precise), and, for $\sigma \in \mathcal{E}_{\rm ext}$, let $[v]_\sigma = v$. Then the following inequality holds:*

$$\Big(\sum_{\sigma\in\mathcal{E}} \frac{1}{h_\sigma} \int_\sigma [v]_\sigma^2\Big)^{1/2} \leq C\ \|v\|_{h,{\rm b}}.$$

where C only depends on θ_0.

Proof. Let σ be an internal face of the mesh. By assumption, the integral of the jump of a discrete function v vanishes either through σ or through a coarse face Σ including σ. Let us first consider the latter situation, which is the most complex; it is encountered when σ is located at an interface between a coarse and a refined zone of the mesh. Let us adopt the notations of Figure 4; the coarse face Σ

includes $n_\Sigma = 2^{d-1}$ refined faces, which we denote by $\sigma_i,\ 1 \leq i \leq n_\Sigma$ and, without loss of generality, let us suppose that

$$v_{\sigma_1} = \min_{1\leq i\leq n_\Sigma} \big\{v_{\sigma_i},\ 1 \leq i \leq n_\Sigma\big\} \text{ and } v_{\sigma_{n_\Sigma}} = \max_{1\leq i\leq n_\Sigma} \big\{v_{\sigma_i},\ 1 \leq i \leq n_\Sigma\big\}.$$

By definition of the discrete space, there exists $\boldsymbol{x}_1 \in \sigma_1$ and $\boldsymbol{x}_{n_\Sigma} \in \sigma_{n_\Sigma}$ such that $v_{|K_1}(\boldsymbol{x}_1) = v_{\sigma_1}$ and $v_{|K_{n_\Sigma}}(\boldsymbol{x}_{n_\Sigma}) = v_{\sigma_{n_\Sigma}}$, respectively (since the mean value of $v_{|K_1}$ (resp. $v_{|K_{n_\Sigma}}$) is v_{σ_1} (resp. $v_{\sigma_{n_\Sigma}}$)). Let us denote by $K_i,\ 1 \leq i \leq n_\Sigma$ the refined cells adjacents to $\sigma_i,\ 1 \leq i \leq n_\Sigma$ and by $\tau_j,\ 1 \leq j \leq n_\tau$, with $n_\tau = 1$ if $d = 2$ and $n_\tau = 4$ if $d = 3$, the faces separating these cells. Still by definition of the discrete space, for $1 \leq j \leq n_\tau$, there exists a point of τ_j where the function v is continuous (since the average of the jump of v across τ_j vanishes). Hence, there exists a piecewise linear path $\mathcal{P}$ included in $\cup_{1\leq i\leq n_\Sigma} K_i$ joining $\boldsymbol{x}_1$ and $\boldsymbol{x}_{n_\Sigma}$ and such that the function v is continuous along $\mathcal{P}$. The mean value v_Σ of v over Σ lies in the interval $[v_{\sigma_1}, v_{\sigma_{n_\Sigma}}]$, so there exists $\boldsymbol{x}^r_\Sigma \in \mathcal{P}$ such that $v(\boldsymbol{x}^r_\Sigma) = v_\Sigma$. Finally, once again by definition of the discrete space, there exists $\boldsymbol{x}^c_\Sigma$ such that $v_{|_K}(\boldsymbol{x}^c_\Sigma) = v_\Sigma$, with K the coarse mesh adjacent to Σ.

Let us consider one of the faces included Σ, let us say σ_1. The point $\boldsymbol{x}^r_\Sigma$ may lie in K_i, $i \neq 1$. However, by the same arguments as previously, there exists a piecewise linear path joining any $\boldsymbol{x}$ of σ to $\boldsymbol{x}^r_\Sigma$ along which v is continuous. Let us suppose that $\boldsymbol{x}^r_\Sigma \in K_2$, and that the path joining $\boldsymbol{x}$ and $\boldsymbol{x}^r_\Sigma$ is made of two segments, which we denote by $(\boldsymbol{x}, \boldsymbol{x}_\tau) \subset K_1$ and $(\boldsymbol{x}_\tau, \boldsymbol{x}^r_\Sigma) \subset K_2$, with $\boldsymbol{x}_\tau$ the point of the face τ where v is continuous. We may now write, making the integration measures apparent in the integrals for the sake of clarity:

$$\int_\sigma [v]^2_\sigma = \int_\sigma \Big(\int_0^1 \boldsymbol{\nabla} v\big((1-\xi)\,\boldsymbol{x}^r_\Sigma + \xi\,\boldsymbol{x}_\tau\big)\cdot(\boldsymbol{x}_\tau - \boldsymbol{x}^r_\Sigma)\,\mathrm{d}\xi + \int_0^1 \boldsymbol{\nabla} v\big((1-\xi)\,\boldsymbol{x}_\tau + \xi\,\boldsymbol{x}\big)\cdot(\boldsymbol{x} - \boldsymbol{x}_\tau)\,\mathrm{d}\xi - \int_0^1 \boldsymbol{\nabla} v_{|_K}\big((1-\xi)\,\boldsymbol{x}_\Sigma + \xi\,\boldsymbol{x}\big)\cdot(\boldsymbol{x} - \boldsymbol{x}_\Sigma)\,\mathrm{d}\xi\Big)^2 \,\mathrm{d}\gamma(\boldsymbol{x}),$$

where $\mathrm{d}\gamma(\boldsymbol{x})$ stands for the measure on the face σ. Hence, $\displaystyle\int_\sigma [v]^2_\sigma \leq 3\,(T_1 + T_2 + T_3)$ with

$$T_1 = \int_\sigma \Big(\int_0^1 \boldsymbol{\nabla} v\big((1-\xi)\,\boldsymbol{x}^r_\Sigma + \xi\,\boldsymbol{x}_\tau\big)\cdot(\boldsymbol{x}_\tau - \boldsymbol{x}^r_\Sigma)\,\mathrm{d}\xi\Big)^2 \,\mathrm{d}\gamma(\boldsymbol{x}),$$

$$T_2 = \int_\sigma \Big(\int_0^1 \boldsymbol{\nabla} v\big((1-\xi)\,\boldsymbol{x}_\tau + \xi\,\boldsymbol{x}\big)\cdot(\boldsymbol{x} - \boldsymbol{x}_\tau)\,\mathrm{d}\xi\Big)^2 \,\mathrm{d}\gamma(\boldsymbol{x}),$$

$$T_3 = \int_\sigma \Big(\int_0^1 \boldsymbol{\nabla} v_{|_K}\cdot\big((1-\xi)\,\boldsymbol{x}_\Sigma + \xi\,\boldsymbol{x}\big)\cdot(\boldsymbol{x} - \boldsymbol{x}_\Sigma)\,\mathrm{d}\xi\Big)^2 \,\mathrm{d}\gamma(\boldsymbol{x}).$$

The Cauchy-Schwarz inequality yields:

$$T_1 \leq h^2_{K_2} \int_\sigma \int_0^1 |\boldsymbol{\nabla} v\big((1-\xi)\,\boldsymbol{x}^r_\Sigma + \xi\,\boldsymbol{x}_\tau\big)|^2\,\mathrm{d}\xi\ \mathrm{d}\gamma(\boldsymbol{x}).$$

The integrand is independent from $\boldsymbol{x}$, and we get:

$$T_1 \leq h^2_{K_2}\ |\sigma|\ \max_{\boldsymbol{x}\in K_2} |\boldsymbol{\nabla} v|^2.$$

Thanks to the properties of the Q_1 mapping, we have

$$\max_{\boldsymbol{x}\in K_2} |\boldsymbol{\nabla} v|^2 \leq C(\theta_0)\ \frac{1}{|K_2|}\ \|\boldsymbol{\nabla} v\|^2_{L^2(K_2)},$$

so, finally:

$$T_1 \leq C(\theta_0)\ \frac{h^2_{K_2}\ |\sigma|}{|K_2|}\ \|\boldsymbol{\nabla} v\|^2_{L^2(K_2)}.$$

For T_2, we have similarly:

$$T_2 \leq h_{K_1}^2 \int_\sigma \int_0^1 |\boldsymbol{\nabla} v\big((1-\xi)\,\boldsymbol{x}_\tau + \xi\,\boldsymbol{x}\big)|^2 \,\mathrm{d}\xi \,\mathrm{d}\gamma(\boldsymbol{x}).$$

Bounding the integrand by $\max_{\boldsymbol{x}\in K_1} |\boldsymbol{\nabla} v|^2$ yields similarly

$$T_2 \leq C(\theta_0)\, \frac{h_{K_1}^2\, |\sigma|}{|K_1|}\, \|\boldsymbol{\nabla} v\|_{L^2(K_1)}^2.$$

Finally, the same arguments yield

$$T_3 \leq C(\theta_0)\, \frac{h_K^2\, |\sigma|}{|K|}\, \|\boldsymbol{\nabla} v\|_{L^2(K)}^2.$$

Gathering the three estimates, we obtain that there exists C depending only on θ_0 such that

$$\frac{1}{h_\sigma} \int_\sigma [v]_\sigma^2 \leq C\Big(\int_K |\boldsymbol{\nabla} v|^2 + \sum_{i=1}^{n_\Sigma} \int_{K_i} |\boldsymbol{\nabla} v|^2\Big).$$

The derivation of this estimate may be easily extended to a path joining $\boldsymbol{x}$ and $\boldsymbol{x}_\Sigma^f$ consisting in three segments, which is the maximum possible value, or simplified to deal with the case where $\boldsymbol{x}_\Sigma^r \in K_1$. The arguments to deal with the case of a face separating two cells of equal level of refinement (*i.e.* a face having no hanging node as vertex) or with external faces may be extracted from the previous derivation (roughly speaking, only the term T_3 appears, twice for an internal face and once for an external one). The conclusion follows by summing over the faces and invoking the fact that the integral of $|\boldsymbol{\nabla} v|^2$ over a given cell appears only a bounded number of times in the sum. ∎

The proof of the following trace lemma is an easy adaptation of a result which can be found in [8, appendix A].

Lemma 4.9. *Let $\mathcal{M}$ be a locally refined mesh of the computational domain Ω and K be a control volume of $\mathcal{M}$, and let σ be one of its faces. Then there exists C, only depending on d, such that the following inequality holds:*

$$\|v\|_{\mathrm{L}^2(\sigma)} \leq C \frac{1}{r_K^{1/2}} \left(\|v\|_{\mathrm{L}^2(K)} + h_K \|\nabla v\|_{\mathrm{L}^2(K)^d}\right), \qquad \forall v \in \mathrm{H}^1(K).$$

We will also need the following Poincaré-Wirtinger inequality, which is proven for any convex domain K in [20, 2].

Lemma 4.10. *For all convex domain K of $\mathbb{R}^d$, $1 \leq d \leq 3$:*

$$\|v - m_K(v)\|_{\mathrm{L}^2(K)} \leq \frac{1}{\pi}\, h_K \|\nabla v\|_{\mathrm{L}^2(K)^d}, \qquad \forall v \in \mathrm{H}^1(K), \tag{4.16}$$

where $m_K(v)$ stands for the mean value of v over K.

We are now in position to prove the following result, which may be seen as a "weighted version" of Lemma 4.8. This result is directly used to bound the consistency error associated to the diffusion term.

Lemma 4.11. *Let $\theta_0 > 0$ and let $\mathcal{M}$ be a locally refined mesh of the computational domain Ω such that $\theta_h \geq \theta_0$, where θ_h is defined by (4.4). We define $\mathcal{E}_\mathrm{c}$ as the set containing:*

- *the internal faces of the mesh which do not have as vertex a hanging node,*
- *the coarse faces,* i.e. *for any hanging node $\boldsymbol{b}$, the subset of a hyperplane made of the union of the faces having $\boldsymbol{b}$ as vertex.*

Let $(a_\Sigma)_{\Sigma\in\mathcal{E}_c}$ be a family of real numbers such that for all $\Sigma\in\mathcal{E}_c$, $|a_\Sigma|\le 1$. Let v be a function of the Rannacher-Turek space V_h associated with $\mathcal{M}$, and, for $\Sigma\in\mathcal{E}_c$ let $[v]_\Sigma$ be the jump of v through Σ. Then the following bound holds:

$$\sum_{\Sigma\in\mathcal{E}_c}\left|\int_\sigma a_\Sigma\ [v]_\Sigma\, g\right| \le C\ h\ \|v\|_{h,b}\ \|\boldsymbol{\nabla} g\|_{\mathrm{L}^2(\Omega)^2},\quad \forall g\in\mathrm{H}^1(\Omega).$$

where the real number C only depends on θ_0 and d.

Proof. Let $\Sigma\in\mathcal{E}_c$ and $v\in V_h$. Since the integral of the jump of v through Σ is zero, we have:

$$\int_\Sigma a_\Sigma\ [v]_\Sigma\, g = \int_\Sigma a_\Sigma\ [v]_\Sigma\,(g-g_\Sigma),$$

where g_Σ is any real number. By the Cauchy-Schwarz inequality in $\mathrm{L}^2(\Sigma)$, we thus get:

$$\sum_{\Sigma\in\mathcal{E}_c}\Big|\int_\Sigma a_\Sigma\ [v]_\Sigma\, g\Big| \le \sum_{\Sigma\in\mathcal{E}_c}\Big(\int_\Sigma [v]_\Sigma^2\Big)^{\frac12}\ \Big(\int_\Sigma (g-g_\Sigma)^2\Big)^{\frac12}.$$

Let us now decompose the integral over Σ in integrals over the faces (in fact, for the coarse faces only), then use the concavity of the square root function, to obtain:

$$\sum_{\Sigma\in\mathcal{E}_c}\Big|\int_\Sigma a_\Sigma\ [v]_\Sigma\, g\Big| \le \sum_{\Sigma\in\mathcal{E}_c}\Big(\sum_{\sigma\subset\Sigma}\Big(\int_\sigma [v]_\sigma^2\Big)^{\frac12}\Big)\ \Big(\int_\Sigma (g-g_\Sigma)^2\Big)^{\frac12}.$$

The discrete Cauchy-Schwarz inequality now yields:

$$\sum_{\Sigma\in\mathcal{E}_c}\Big|\int_\Sigma a_\Sigma\ [v]_\Sigma\, g\Big| \le \Big(\sum_{\sigma\in\mathcal{E}}\frac{1}{h_\sigma}\int_\sigma [v]_\sigma^2\,\mathrm{d}\gamma\Big)^{\frac12}\ \underbrace{\left(\sum_{\Sigma\in\mathcal{E}_c} h_\Sigma\int_\Sigma (g-g_\Sigma)^2\right)^{\frac12}}_{T_1},$$

where h_Σ stands for the sum of the diameters of the faces included in Σ (which is equal to the diameter of Σ in two dimensions, and lower than four times this diameter in three dimensions). By Lemma 4.8, the first term of the latter product is bounded by $C(\theta_0)\,\|v\|_{h,b}$. For the second one, for $\Sigma\in\mathcal{E}_c$, let K_Σ be a cell of the mesh having Σ as a whole side (two choices are possible for a standard face, and only one for a coarse one). Applying the trace lemma 4.9, we get:

$$T_1^2 \le C(d)\sum_{\Sigma\in\mathcal{E}_c}\frac{h_\Sigma}{r_{K_\Sigma}}\ \left(\|g-g_\Sigma\|^2_{\mathrm{L}^2(K_\Sigma)} + h_{K_\Sigma}^2\|\nabla g\|^2_{\mathrm{L}^2(K_\Sigma)^d}\right).$$

Choosing for g_Σ the mean value of g on K_Σ and using (4.16), we thus get:

$$T_1^2 \le C(d)\sum_{\Sigma\in\mathcal{E}_c}(1+\frac{1}{\pi^2})\,\frac{h_\Sigma}{r_{K_\Sigma}}h_{K_\Sigma}^2\|\nabla g\|^2_{\mathrm{L}^2(K_\Sigma)^d} \le C(d,\theta_0)\ h^2\sum_{\Sigma\in\mathcal{E}_c}\|\nabla g\|^2_{\mathrm{L}^2(K_\Sigma)^d}.$$

The result follows by observing that the H^1 semi-norm of g on a given cell K of the mesh appears at most $2d$ (the maximum number of sides of a cell K) times in the summation. ∎

Finally, we now give two technical corollaries of Lemmas 4.9 and 4.10; they both compare different mean values of functions of $\mathrm{H}^1(\Omega)$.

Lemma 4.12. *Let $\mathcal{M}$ be a locally refined mesh of the computational domain Ω; let $K\in\mathcal{M}$ and let D be a subset of K. For all $v\in\mathrm{H}^1(K)$, we denote $m_K(v)$ and $m_D(v)$ the mean values of v on K and D respectively. Then:*

$$|m_K(v)-m_D(v)| \le \frac{1}{\pi\,|D|^{\frac12}}\ h_K\ \|\boldsymbol{\nabla} v\|_{\mathrm{L}^2(K)^d},\qquad \forall v\in\mathrm{H}^1(K).$$

Proof. By the Cauchy-Schwarz inequality, we have:

$$|m_K(v) - m_D(v)| = \frac{1}{|D|}\left|\int_D \big(v - m_K(v)\big)\right| \leq \frac{1}{|D|^{\frac{1}{2}}}\ \|v - m_K(v)\|_{\mathrm{L}^2(D)}.$$

Thus, since D is a subset of K, we have:

$$|m_K(v) - m_D(v)| \leq \frac{1}{|D|^{\frac{1}{2}}}\ \|v - m_K(v)\|_{\mathrm{L}^2(K)},$$

and we conclude by Lemma 4.10, since K is convex. ∎

Lemma 4.13. *Let $\theta_0 > 0$ and let $\mathcal{M}$ be a locally refined mesh of the computational domain Ω such that $\theta_h \leq \theta_0$, with θ_h defined by (4.4). Let $K \in \mathcal{M}$ be a control volume and let σ be a face of K. For all $v \in \mathrm{H}^1(K)$, we denote $m_\sigma(v)$ and $m_K(v)$ the mean values of v on σ and K respectively. Then, there exists C, only depending on d and θ_0 such that:*

$$|m_\sigma(v) - m_K(v)| \leq \frac{C}{r_K^{d/2}}\ h_K \|\nabla v\|_{\mathrm{L}^2(K)^d}, \qquad \forall v \in \mathrm{H}^1(K). \tag{4.17}$$

Proof. We have $|m_\sigma(v) - m_K(v)| \leq |\sigma|^{-1}\int_\sigma |v - m_K(v)| \leq |\sigma|^{-1/2}\|v - m_K(v)\|_{\mathrm{L}^2(\sigma)}$ by the Cauchy-Schwarz inequality. Invoking successively Lemma 4.9 and Lemma 4.10 and using the regularity of the mesh yields the result. ∎

4.4.2. *The interpolation operator*

We define by r_h the following interpolation operator:

$$r_h : \left|\begin{array}{lcl} \mathrm{H}^1_0(\Omega) & \longrightarrow & V_h \\ v & \mapsto & r_h v(\boldsymbol{x}) = \displaystyle\sum_{\sigma\in\mathcal{E}} |\sigma|^{-1}\left(\int_\sigma v\,\mathrm{d}\gamma\right)\zeta_\sigma(\boldsymbol{x}). \end{array}\right. \tag{4.18}$$

The stability and approximation properties of r_h are given in the following lemma.

Lemma 4.14. *Let $\theta_0 > 0$ and let $\mathcal{M}$ be a locally refined mesh of the computational domain Ω such that $\theta_h \leq \theta_0$, with θ_h defined by (4.4). There exists C_1 and C_2 only depending on θ_0 such that*

(1) *Stability:*

$$\forall v \in \mathrm{H}^1_0(\Omega), \quad \|r_h v\|_{\mathrm{L}^2(\Omega)} + \|r_h v\|_{h,\mathrm{b}} \leq C_1\ \|\boldsymbol{\nabla} v\|_{\mathrm{L}^2(\Omega)^d}.$$

(2) *Approximation properties:*

$$\forall v \in \mathrm{H}^1_0(\Omega)\cap\mathrm{H}^2(\Omega),\ \forall K \in \mathcal{M},$$
$$\|v - r_h v\|_{\mathrm{L}^2(K)} + h_K\ \|\boldsymbol{\nabla}(v - r_h v)\|_{\mathrm{L}^2(K)^d} \leq C_2\, h_K(h_K + \alpha_K)\ \|v\|_{\mathrm{H}^2(K)}.$$

Proof. The stability property follows from usual estimates on the shape functions and from the trace lemma 4.9. We prove the approximation property. If there is no hanging node on the faces of K, r_h is the usual Rannacher-Turek interpolation operator, and the result is known. In the other case, for $d = 2$, let us suppose that an initial face Σ of K has been split: $\Sigma = \sigma_1 \cup \sigma_2$. Let $v \in \mathrm{H}^1_0(\Omega)$. Then we get for the part of the expansion of $r_h v$ associated with σ_1 and σ_2, let us say $r_h v^{\sigma_1\cup\sigma_2}$:

$$\begin{aligned} r_h v^{\sigma_1\cup\sigma_2}|_K &= \frac{1}{|\sigma_1|}\Big(\int_{\sigma_1} v\,\mathrm{d}\gamma\Big)\ \frac{|\sigma_1|}{|\Sigma|}\ \zeta_\Sigma(\boldsymbol{x}) + \frac{1}{|\sigma_2|}\Big(\int_{\sigma_2} v\,\mathrm{d}\gamma\Big)\ \frac{|\sigma_2|}{|\Sigma|}\ \zeta_\Sigma(\boldsymbol{x}) \\ &= \frac{1}{|\Sigma|}\ \Big(\int_\Sigma v\,\mathrm{d}\gamma\Big)\ \zeta_\Sigma(\boldsymbol{x}). \end{aligned}$$

Once again, we recognize the usual Rannacher-Turek interpolation operator. The same arguments readily extend to the 3D case. ∎

Remark 4.15 (*inf-sup* condition on locally refined meshes)**.** The same computation shows that, as for the usual Rannacher-Turek approximation on regular meshes, the operator r_h, or, more precisely, its natural extension to vector-valued functions, is a Fortin operator (*i.e.* continuous from $\mathrm{H}^1_0(\Omega)^d$ to V_h^d endowed with the H^1-broken norm and such that $\int_\Omega q\,\mathrm{div}(\boldsymbol{u} - r_h\boldsymbol{u}) = 0$ for any discrete pressure function q); this implies that the *inf-sup* condition is satisfied by the pair of velocity and pressure approximation spaces also on locally refined meshes.

4.4.3. *Estimates on the discrete convective term*

The form b_h is a discretization of the convection term on the cells of the dual mesh. The analysis of the scheme actually requires an equivalent (or nearly equivalent) re-formulation of the form b_h on the cells of the primal mesh $\mathcal{M}$, that makes use of the primal fluxes $F_{K,\sigma}(\boldsymbol{w})$. Indeed, contrary to the dual fluxes $F_{\sigma,\epsilon}(\boldsymbol{w})$, the expression of $F_{K,\sigma}(\boldsymbol{w})$ with respect to the convection field $\boldsymbol{w}$ is quite simple (see (4.7)). This motivates the introduction of the following auxiliary form:

$$\widetilde{b}_h(\boldsymbol{w},u,v) = \sum_{K\in\mathcal{M}} v_K \sum_{\sigma\in\mathcal{E}(K)} F_{K,\sigma}(\boldsymbol{w})\; u_\sigma, \qquad u,v\in V_h,$$

where $v_K = \sum_{\sigma\in\mathcal{E}(K)} \xi_K^\sigma\, v_\sigma$ is a convex combination of $(v_\sigma)_{\sigma\in\mathcal{E}(K)}$, where the coefficient ξ_K^σ is equal to $1/(2d)$, when σ has not been split, or $1/(2^d d)$ otherwise. The following lemma provides a bound of the error made when replacing b_h by $\widetilde{b}_h$. It may be seen as a simplified version of a slightly more general result, dealing with density-dependent fluxes $F_{K,\sigma}$, which may be found in [16]; we however give its proof, for the sake of completeness.

Lemma 4.16. *Let $\theta_0 > 0$ and let $\mathcal{M}$ be a locally refined mesh of the computational domain Ω such that $\theta_h \le \theta_0$, with θ_h defined by* (4.4)*. There exists C, only depending on θ_0 such that:*

$$|\widetilde{b}_h(\boldsymbol{w},u,v) - b_h(\boldsymbol{w},u,v)| \le C\,h\,\|\boldsymbol{w}\|_{\mathrm{L}^\infty(\Omega)^d}\;\|u\|_{h,\mathrm{b}}\;\|v\|_{h,\mathrm{b}}, \qquad \forall u,v\in V_h. \tag{4.19}$$

Proof. Denote $R = b_h(\boldsymbol{w},u,v) - \widetilde{b}_h(\boldsymbol{w},u,v)$. In the expression (4.10) of $b_h(\boldsymbol{w},u,v)$, for $\sigma = K|L$, let us split the sum over the fluxes through the faces of D_σ in the sum over the dual faces, on one side, included in K and, on the other side, included in L. We get by conservativity (*i.e.* using $F_{K,\sigma}(\boldsymbol{w}) = -F_{L,\sigma}(\boldsymbol{w})$):

$$b_h(\boldsymbol{w},u,v) = \sum_{K\in\mathcal{M}}\sum_{\sigma\in\mathcal{E}(K)} v_\sigma\; T_{K,\sigma}, \quad \text{with} \quad T_{K,\sigma} = F_{K,\sigma}(\boldsymbol{w})\; u_\sigma + \sum_{\substack{\epsilon\in\tilde{\mathcal{E}}(D_\sigma),\ \epsilon\subset K,\\ \epsilon = D_\sigma|D'_\sigma}} F_{\sigma,\epsilon}(\boldsymbol{w})\;\frac{u_\sigma + u_{\sigma'}}{2}.$$

Let us write $b_h(\boldsymbol{w},u,v) = T_1 + T_2$ with:

$$T_1 = \sum_{K\in\mathcal{M}} v_K \sum_{\sigma\in\mathcal{E}(K)} T_{K,\sigma}, \qquad T_2 = \sum_{K\in\mathcal{M}}\sum_{\sigma\in\mathcal{E}(K)} (v_\sigma - v_K) T_{K,\sigma}.$$

By the conservativity assumption of the dual fluxes $(H2)$ (see Definition 3.1), we remark that $T_1 = \widetilde{b}_h(\boldsymbol{w},u,v)$ so that $R = T_2$. Using now $(H1)$, we write $R = R_1 + R_2$ with:

$$R_1 = \sum_{K\in\mathcal{M}}\sum_{\sigma\in\mathcal{E}(K)} (v_\sigma - v_K)\Big(\sum_{\substack{\epsilon\in\tilde{\mathcal{E}}(D_\sigma),\ \epsilon\subset K,\\ \epsilon = D_\sigma|D'_\sigma}} F_{\sigma,\epsilon}(\boldsymbol{w})\;\frac{u_{\sigma'} - u_\sigma}{2}\Big),$$

$$R_2 = \sum_{K\in\mathcal{M}} \sum_{\sigma\in\mathcal{E}(K)} (v_\sigma - v_K)\ u_\sigma\ \xi_K^\sigma\ \Big(\sum_{\sigma'\in\mathcal{E}(K)} F_{K,\sigma'}(\boldsymbol{w})\Big).$$

Since $\boldsymbol{w}$ is assumed to be divergence-free, the last sum in R_2 (and so R_2 itself) vanishes. The assumption $(H3)$ yields $|F_{\sigma,\epsilon}(\boldsymbol{w})| \le C\|\boldsymbol{w}\|_{\mathrm{L}^\infty(\Omega)^d}\ h_K^{d-1}$. As a consequence, since v_K is a convex combination of the $(v_\sigma)_{\sigma\in\mathcal{E}(K)}$, we have for any $K\in\mathcal{M}$:

$$\Big|\sum_{\sigma\in\mathcal{E}(K)} (v_\sigma - v_K)\Big(\sum_{\substack{\epsilon\in\tilde{\mathcal{E}}(D_\sigma),\ \epsilon\subset K,\\ \epsilon = D_\sigma|D'_\sigma}} F_{\sigma,\epsilon}(\boldsymbol{w})\ \frac{u_{\sigma'}-u_\sigma}{2}\Big)\Big| \le$$

$$C\|\boldsymbol{w}\|_{\mathrm{L}^\infty(\Omega)^d} h \sum_{\sigma,\sigma',\sigma'',\sigma'''\in\mathcal{E}(K)} h_K^{d-2}\ |v_\sigma - v_{\sigma'}|\ |u_{\sigma''} - u_{\sigma'''}|,$$

and, for $\sigma,\ \sigma'\in\mathcal{E}(K)$, the quantity $|u_\sigma - u_{\sigma'}|$ (or $|v_\sigma - v_{\sigma'}|$) appears in the sum a finite number of times which depends of the dimension d. Hence, by the Cauchy-Schwarz inequality and invoking Lemma 4.6:

$$|R_1| \le C\ h\ \|\boldsymbol{w}\|_{\mathrm{L}^\infty(\Omega)^d}\ \|u\|_{h,\mathrm{fv}}\ \|v\|_{h,\mathrm{fv}} \le C'\ h\ \|\boldsymbol{w}\|_{\mathrm{L}^\infty(\Omega)^d}\ \|u\|_{h,\mathrm{b}}\ \|v\|_{h,\mathrm{b}}.$$

■

Remark 4.17. The fact that the term R_2 vanishes is specific to a divergence-free advection field, and this may lead to think that the lemma result does not hold when $\boldsymbol{w}$ is an approximation of the momentum field and the density varies in space and time. In fact, the above proof extends to cope with this case by remarking that, by definition of v_K, $\sum_{\sigma\in\mathcal{E}(K)}\xi_K^\sigma\ (v_\sigma - v_K) = 0$, so u_σ may be replaced by $u_\sigma - u_K$ in the expression of R_2. The desired bound then follows by arguments similar to the majoration of R_1.

4.4.4. *Proof of Theorem 4.3*

Let u be the solution of the continuous problem (4.2) which we assume to belong to $\mathrm{H}_0^1(\Omega)\cap\mathrm{H}^2(\Omega)$ and let u_h be the solution of the scheme (4.8). By the triangle inequality, we have $\|u_h - u\|_{h,\mathrm{b}} \le \|u_h - r_h u\|_{h,\mathrm{b}} + \|r_h u - u\|_{h,\mathrm{b}}$ where r_h is the interpolation operator defined in (4.18). The approximation property stated in Lemma 4.14 yields:

$$\|r_h u - u\|_{h,\mathrm{b}} = \Big(\sum_{K\in\mathcal{M}} \|\boldsymbol{\nabla}(u - r_h u)\|^2_{\mathrm{L}^2(K)^d}\Big)^{\frac12} \le C_2(h+\alpha_h)\ \|u\|_{\mathrm{H}^2(\Omega)}. \tag{4.20}$$

To complete the proof, we now have to estimate the quantity $\|u_h - r_h u\|_{h,\mathrm{b}}$. To this purpose, we introduce $\|v\|_h^2 = \mathcal{A}_h(v,v) = (v,v)_h + \|v\|_{h,\mathrm{b}}^2$, which defines a norm on V_h that controls the broken Sobolev H^1-norm $\|v\|_{h,\mathrm{b}}$. Hence, we have:

$$\|u_h - r_h u\|_{h,\mathrm{b}} \le \|u_h - r_h u\|_h \le \sup_{v\in V_h} \frac{\mathcal{A}_h(u_h - r_h u, v)}{\|v\|_h}.$$

Since u_h is the solution of the scheme (4.8), we have $\mathcal{A}_h(u_h, v) = (f, v)$ for all $v\in V_h$. In addition, u belongs to $\mathrm{H}_0^1(\Omega)\cap\mathrm{H}^2(\Omega)$, which implies that the strong form of the continuous problem, *i.e.* Equation (4.1a), holds in $\mathrm{L}^2(\Omega)$ and thus, since $V_h\subset\mathrm{L}^2(\Omega)$:

$$(u,v) + (\mathrm{div}(u\boldsymbol{w}), v) - (\boldsymbol{\Delta}u, v) = (f,v), \qquad \forall v\in V_h.$$

As a consequence, we have $\mathcal{A}_h(u_h - r_h u, v) = T_1 + T_2 + T_3$ where:

$$T_1 = (u,v) - (r_h u, v)_h, \quad T_2 = (\mathrm{div}(u\boldsymbol{w}), v) - b_h(\boldsymbol{w}, r_h u, v), \quad T_3 = (-\boldsymbol{\Delta}u, v) - a_h(r_h u, v).$$

Reaction term - Let us recall that, for $v \in V_h$, we have defined $v_{\rm c}$ as the piecewise constant function over each diamond cell and which takes the value v_σ over D_σ, for $\sigma \in \mathcal{E}$. The term T_1 then reads:

$$T_1 = (u,v) - ((r_h u)_{\rm c}, v_{\rm c}) = \frac{1}{2}(u + (r_h u)_{\rm c}, v - v_{\rm c}) + \frac{1}{2}(u - r_h u, v + v_{\rm c}) + \frac{1}{2}(r_h u - (r_h u)_{\rm c}, v + v_{\rm c}).$$

Then, invoking the stability and approximation properties stated in Lemma 4.14 and using Lemma 4.7 to bound $\|(r_h u)_{\rm c}\|_{L^2(\Omega)}$, $\|v_{\rm c}\|_{L^2(\Omega)}$ and $\|v - v_{\rm c}\|_{L^2(\Omega)}$, we obtain

$$|T_{1,2}| \leq Ch \ \|\boldsymbol{\nabla} u\|_{\mathrm{L}^2(\Omega)^d} \ \|v\|_h.$$

Convection term - Let us now turn to T_2. We may write $T_2 = T_{2,1} + R$ where:

$$T_{2,1} = (\mathrm{div}(u\boldsymbol{w}), v) - \widetilde{b}_h(\boldsymbol{w}, r_h u, v), \qquad R = \widetilde{b}_h(\boldsymbol{w}, r_h u, v) - b_h(\boldsymbol{w}, r_h u, v).$$

Applying Lemma 4.16 and invoking the stability property of Lemma 4.14, we get

$$|R| \leq C\, h \ \|\boldsymbol{w}\|_{\mathrm{L}^\infty(\Omega)^d} \ \|\boldsymbol{\nabla} u\|_{\mathrm{L}^2(\Omega)^d} \|v\|_h.$$

For the term $T_{2,1}$, we have:

$$T_{2,1} = (\mathrm{div}(u\boldsymbol{w}), v - v_{\rm m}) - \sum_{K\in\mathcal{M}} v_K \sum_{\sigma\in\mathcal{E}(K)} \int_\sigma (u - (r_h u)_\sigma) \boldsymbol{w}\cdot\boldsymbol{n}_{K,\sigma},$$

where $v_{\rm m}$ stands for the piecewise constant function over each cell K and equal to v_K. By the Cauchy-Schwarz inequality and Lemma 4.7, the first term at the right-hand side of this relation may be bounded as follow:

$$|(\mathrm{div}(u\boldsymbol{w}), v - v_{\rm m})| \leq C\, h \ \|\boldsymbol{w}\|_{\mathrm{L}^\infty(\Omega)^d} \ \|u\|_{\mathrm{H}^1(\Omega)} \ \|v\|_h.$$

For the second term, we first remark that:

$$\begin{aligned}
\Big|\int_\sigma \big(u - (r_h u)_\sigma\big) \ \boldsymbol{w}\cdot\boldsymbol{n}_{K,\sigma}\Big| &\leq \|\boldsymbol{w}\|_{\mathrm{L}^\infty(\Omega)^d} \ |\sigma|^{1/2} \ \|u - m_\sigma(u)\|_{\mathrm{L}^2(\sigma)} \\
&\leq \|\boldsymbol{w}\|_{\mathrm{L}^\infty(\Omega)^d} \ \big(|\sigma|^{1/2} \ \|u - m_K(u)\|_{\mathrm{L}^2(\sigma)} + |\sigma| \ |m_K(u) - m_\sigma(u)|\big) \\
&\leq C \ \|\boldsymbol{w}\|_{\mathrm{L}^\infty(\Omega)^d} \ h_K^{d/2} \ \|\boldsymbol{\nabla} u\|_{\mathrm{L}^2(K)^d},
\end{aligned}$$

by the regularity of the mesh and Lemmas 4.9, 4.10 and 4.13. Hence, reordering the summations, we thus get (invoking the boundary conditions to exclude the external faces from the summation):

$$\begin{aligned}
&\Big|\sum_{K\in\mathcal{M}} v_K \sum_{\sigma\in\mathcal{E}(K)} \int_\sigma (u - (r_h u)_\sigma) \ \boldsymbol{w}\cdot\boldsymbol{n}_{K,\sigma}\Big| \\
&\quad\leq C \ \|\boldsymbol{w}\|_{\mathrm{L}^\infty(\Omega)^d} \ h \sum_{\substack{\sigma\in\mathcal{E}_{\rm int}\\ \sigma = K|L}} h_K^{d/2-1} \ \|\boldsymbol{\nabla} u\|_{\mathrm{L}^2(K)^d} \ |v_K - v_L| \\
&\quad\leq C \ \|\boldsymbol{w}\|_{\mathrm{L}^\infty(\Omega)^d} \ h \Big(\sum_{\sigma\in\mathcal{E}_{\rm int}} \|\boldsymbol{\nabla} u\|^2_{\mathrm{L}^2(K)^d}\Big)^{1/2} \Big(\sum_{\substack{\sigma\in\mathcal{E}_{\rm int}\\ \sigma = K|L}} h_K^{d-2} \, |v_K - v_L|^2\Big)^{\frac{1}{2}} \\
&\quad\leq C\, 2^d\, d \ \|\boldsymbol{w}\|_{\mathrm{L}^\infty(\Omega)^d} \ \|\boldsymbol{\nabla} u\|_{\mathrm{L}^2(\Omega)^d} \ h \Big(\sum_{\substack{\sigma\in\mathcal{E}_{\rm int}\\ \sigma = K|L}} h_K^{d-2} |v_K - v_L|^2\Big)^{\frac{1}{2}},
\end{aligned}$$

with $2^d\, d$ the maximum number of the faces of the cells, so the maximum nuber of times a cell K may appear in the sum. Since v_K is a convex combination of $(v_\sigma)_{\sigma\in\mathcal{E}(K)}$, we have, possibly splitting

a difference $v_\sigma - v_{\sigma'}$ as $v_\sigma - v_{\sigma'} = (v_\sigma - v_{K|L}) - (v_{\sigma'} - v_{K|L})$ if σ and σ' are not faces of the same element:

$$|v_K - v_L| \leq 2 \sum_{\sigma,\sigma' \in \mathcal{E}(K)} |v_\sigma - v_{\sigma'}| + 2 \sum_{\sigma,\sigma' \in \mathcal{E}(L)} |v_\sigma - v_{\sigma'}|.$$

Therefore, since the number of faces of an element is bounded, there exists a fixed real number C such that:

$$\Big(\sum_{\substack{\sigma \in \mathcal{E}_{\rm int} \\ \sigma = K|L}} h_K^{d-2} |v_K - v_L|^2 \Big)^{1/2} \leq C \, \Big(\sum_{K \in \mathcal{M}} h_K^{d-2} \sum_{\sigma,\sigma' \in \mathcal{E}(K)} |v_\sigma - v_{\sigma'}|^2 \Big)^{1/2},$$

and, invoking Lemma 4.6, this sum is bounded by $\|v\|_{h,\rm b}$, and thus by $\|v\|_h$. We finally get:

$$|T_{2,1}| \leq C \; h \; \|\boldsymbol{w}\|_{\mathrm{L}^\infty(\Omega)^d} \; \|u\|_{\mathrm{H}^1(\Omega)} \; \|v\|_h,$$

where C only depends on θ_0. Combining this relation with the bound obtained for R yields that T_2 satisfies the same inequality.

Diffusion term - We finally turn to T_3. Integrating by parts, we get:

$$T_3 = \sum_{K \in \mathcal{M}} \int_K (\boldsymbol{\nabla} u - \boldsymbol{\nabla} r_h u) \cdot \boldsymbol{\nabla} v - \sum_{K \in \mathcal{M}} \sum_{\sigma \in \mathcal{E}(K)} \int_\sigma v \, \boldsymbol{\nabla} u \cdot \boldsymbol{n}_{K,\sigma}.$$

Thanks to Lemma 4.14, we obtain for the first term, using first the Cauchy-Schwarz inequality in $\mathrm{L}^2(K)$ and then the discrete Cauchy-Schwarz inequality:

$$\Big| \sum_{K \in \mathcal{M}} \int_K (\boldsymbol{\nabla} u - \boldsymbol{\nabla} r_h u) \cdot \boldsymbol{\nabla} v \Big| \leq C \, (h + \alpha_h) \; \|u\|_{\mathrm{H}^2(\Omega)} \; \|v\|_{h,\rm b} \leq C \, (h + \alpha_h) \; \|u\|_{\mathrm{H}^2(\Omega)} \; \|v\|_h.$$

Reordering the sums in the second term yields:

$$\sum_{K \in \mathcal{M}} \sum_{\sigma \in \mathcal{E}(K)} \int_\sigma v \, \boldsymbol{\nabla} u \cdot \boldsymbol{n}_{K,\sigma} = \sum_{\sigma \in \mathcal{E}} \int_\sigma [v]_\sigma \, \boldsymbol{\nabla} u \cdot \boldsymbol{n}_\sigma,$$

where $[v]_\sigma$ and $\boldsymbol{n}_\sigma$ stand for the jump of v through σ and a normal vector to σ, with the same orientation. Since, on a coarse face (*i.e.* the subset of a hyperplane which consists in the union of the faces sharing the same hanging node), the normal is the same, we can group the terms in the above sum to obtain, with the notations of Lemma 4.11:

$$\sum_{K \in \mathcal{M}} \sum_{\sigma \in \mathcal{E}(K)} \int_\sigma v \, \boldsymbol{\nabla} u \cdot \boldsymbol{n}_{K,\sigma} = \sum_{\Sigma \in \mathcal{E}_{\rm c}} \int_\Sigma [v]_\Sigma \, \boldsymbol{\nabla} u \cdot \boldsymbol{n}_\Sigma.$$

We thus may apply Lemma 4.11 for $i = 1, .., d$ with $a_\Sigma = \boldsymbol{n}_\Sigma^i$ and $g = \partial_i u$, and we get:

$$\Big| \sum_{K \in \mathcal{M}} \sum_{\sigma \in \mathcal{E}(K)} \int_\sigma v \, \boldsymbol{\nabla} u \cdot \boldsymbol{n}_{K,\sigma} \Big| \leq C \, h \, \|u\|_{\mathrm{H}^2(\Omega)} \; \|v\|_h,$$

which provides the bound for T_3 which we are seeking.

Conclusion - Collecting the bounds for T_1, T_2 and T_3, we obtain that $\|u_h - r_h u\|_{h,\rm b} \leq C \, (h + \alpha_h) \; \|u\|_{\mathrm{H}^2(\Omega)}$ where C only depends on $\boldsymbol{w}$, Ω and θ_0. Combining this with equation (4.20) concludes the proof of Theorem 4.3.

5. **Numerical tests**

The convection and diffusion operators have been implemented in the CALIF^{3}S free component library for fluid flows computation developed at IRSN [5], in the prediction step of pressure correction algorithms used for quasi-incompressible, barotropic or non-barotropic compressible flows. Here, we address the asymptotic model for low Mach number flows [19], which consists in a system of a vector and two scalar balance partial differential equations, corresponding to the momentum, mass and energy balance, respectively:

$$\partial_t(\rho u_i) + \mathrm{div}(\rho u_i \boldsymbol{u}) - \mathrm{div}(\boldsymbol{\tau}(\boldsymbol{u}))_i + \partial_i p = 0, \qquad 1 \leq i \leq d, \tag{5.1}$$

$$\partial_t \rho + \mathrm{div}(\rho \boldsymbol{u}) = 0, \tag{5.2}$$

$$\partial_t(\rho c_p \vartheta) + \mathrm{div}(\rho c_p \vartheta \boldsymbol{u}) - \mathrm{div}(\lambda \boldsymbol{\nabla}\vartheta) = \frac{d}{dt} P_{th}, \tag{5.3}$$

where ϑ stands for the temperature, and c_p and λ are known positive real numbers (the heat capacity and the temperature diffusion coefficient, respectively). We recall that the shear stress tensor $\boldsymbol{\tau}$ reads:

$$\boldsymbol{\tau}(\boldsymbol{u}) = \mu(\boldsymbol{\nabla}\boldsymbol{u} + \boldsymbol{\nabla}^t\boldsymbol{u}) - \frac{2\mu}{3}\,\mathrm{div}\boldsymbol{u}\, I, \quad \mu > 0.$$

The pressure P_{th} is referred to as "the thermodynamical pressure", and is supposed to depend only on time, or, in other words, to be constant in space, which has for effect to filter out the acoustic contributions from the flow field. It is involved in the equation of state which complements the system of balance equations:

$$P_{th} = \rho R \vartheta, \tag{5.4}$$

where R stands for a constant specific to the gas under consideration. Initial conditions must be provided for $\boldsymbol{u}$, ϑ and P_{th}, and the equation of state yields the density at the initial state. For a closed volume (*i.e.* when homogeneous Dirichlet boundary conditions are prescribed on the whole boundary), the thermodynamical pressure at time t may be obtained from the temperature field by the overall mass balance:

$$\int_\Omega \rho(\boldsymbol{x},t)\ \mathrm{d}\boldsymbol{x} = P_{th}(t) \int_\Omega \frac{1}{R\vartheta(\boldsymbol{x},t)}\ \mathrm{d}\boldsymbol{x} = P_{th,0} \int_\Omega \frac{1}{R\vartheta_0(\boldsymbol{x})}\ \mathrm{d}\boldsymbol{x},$$

with $P_{th,0}$ and ϑ_0 the initial thermodynamical pressure and temperature field. Getting rid of (5.4) and setting $\rho = 1$, the first two equations of System (5.1) boil down to the usual incompressible Navier-Stokes equations. We address two tests here: the first one consists in an incompressible problem which admits a known solution and the second one is a classical benchmark for low Mach natural convection flows. Before presenting the numerical results, we first specify the time-marching algorithm used to solve System (5.1), together with the space discretization of some differential terms which has not been encountered until now.

5.1. **The scheme**

5.1.1. *General form of the scheme*

Let us consider a uniform partition $0 = t_0 < t_1 < \ldots < t_N = T$ of the time interval $(0,T)$, and let $\delta t = t_{n+1} - t_n$ for $0 \leq n \leq N-1$ be the constant time step. The temperature is approximated by a finite volume technique based on the primal mesh, so the unknowns of the scheme are $(\rho_K^n)_{K\in\mathcal{M}} \subset \mathbb{R}$, $(\vartheta_K^n)_{K\in\mathcal{M}} \subset \mathbb{R}$, $P_{th}^n \in \mathbb{R}$ and $(\boldsymbol{u}_\sigma)_{\sigma\in\mathcal{E}} \subset \mathbb{R}^d$, for $0 \leq n \leq N$. The initial discrete pressure and velocity

are defined as follows:

$$\begin{aligned} &\rho_K^{-1} = \frac{1}{|K|}\int_K \rho_0(\boldsymbol{x})\,\mathrm{d}\boldsymbol{x}, \quad \vartheta_K^0 = \frac{1}{|K|}\int_K \vartheta_0(\boldsymbol{x})\,\mathrm{d}\boldsymbol{x}, \quad p_K^0 = 0, && K\in\mathcal{M},\\ &\boldsymbol{u}_\sigma^0 = \frac{1}{|\sigma|}\int_\sigma \boldsymbol{u}_0(\boldsymbol{x})\,\mathrm{d}\gamma(\boldsymbol{x}), && \sigma\in\mathcal{E}_{\rm int}. \end{aligned} \tag{5.5}$$

The Dirichlet boundary conditions for the velocity are taken into account by setting $\boldsymbol{u}_\sigma^n$ to the mean value of $\boldsymbol{u}_{\partial\Omega}$ over σ, for all $\sigma\in\mathcal{E}_{\rm ext}$ and all n in $\{0,1,..,N\}$. The value of the initial density $(\rho_K^0)_{K\in\mathcal{M}}$ is obtained from $(\rho_K^{-1})_{K\in\mathcal{M}}$ by solving the discrete mass balance with the initial velocity, to allow to build a monotone (for the temperature) or kinetic energy preserving (for the velocity) convection operator (see Equation (5.6e) in the algorithm below). Finally, T_{th}^0 is obtained by the equation of state linking ρ^0 and ϑ^0 (see Equation (5.6b)).

The time-marching technique implemented in CALIF^{3}S is a fractional step algorithm, which consists in the following three steps: (*i*) solution of the energy balance, (*ii*) computation of the thermodynamical pressure and update of the density by the equation of state and (*iii*) solution of the momentum and balance equations by a pressure correction scheme [25, 6, 12], which is itself a two-steps algorithm. Let us assume that $(\vartheta^n)_{K\in\mathcal{M}}$, P_{th}^{n-1}, P_{th}^n, $(\rho_K^{n-1})_{K\in\mathcal{M}}$, $(\rho_K^n)_{K\in\mathcal{M}}$, $(p_K^n)_{K\in\mathcal{M}}$ and $(\boldsymbol{u}_\sigma^n)_{\sigma\in\mathcal{E}_{\rm int}}$ are known families of real numbers. Then a time step computation consists in finding $(\vartheta^{n+1})_{K\in\mathcal{M}}$, P_{th}^{n+1}, $(p_K^{n+1})_{K\in\mathcal{M}}$ and $(\boldsymbol{u}_\sigma^{n+1})_{\sigma\in\mathcal{E}_{\rm int}}$ through the following algorithm:

Energy balance – Find $(\vartheta_K^{n+1})_{K\in\mathcal{M}}$ such that:

$$\frac{1}{\delta t}(\rho_K^n\vartheta_K^{n+1} - \rho_K^{n-1}\vartheta_K^n) + \frac{1}{|K|}\sum_{\sigma\in\mathcal{E}(K)} F_{K,\sigma}^{n+1}\,\vartheta_\sigma^n - \left(\mathrm{div}(\lambda\boldsymbol{\nabla}\vartheta^{n+1})\right)_K^{n+1} = 0, \quad K\in\mathcal{M}, \tag{5.6a}$$

P_{th} and density update – Compute P_{th}^{n+1} and $(\rho_K^{n+1})_{K\in\mathcal{M}}$ by:

$$P_{th}^{n+1}\sum_{K\in\mathcal{M}}\frac{|K|}{R\,\vartheta_K^{n+1}} = \sum_{K\in\mathcal{M}}|K|\,\rho_K^{-1} \quad\text{and}\quad \rho_K^{n+1} = \frac{P_{th}^{n+1}}{R\,\vartheta_K^{n+1}}, \qquad K\in\mathcal{M}, \tag{5.6b}$$

Prediction step – Find $(\boldsymbol{u}_\sigma^{n+\frac12})_{\sigma\in\mathcal{E}_{\rm int}}$ such that:

$$\begin{aligned} &\frac{1}{\delta t}(\rho_\sigma^n\boldsymbol{u}_\sigma^{n+\frac12} - \rho_\sigma^{n-1}\boldsymbol{u}_\sigma^n) + \frac{1}{|D_\sigma|}\sum_{\epsilon\in\tilde{\mathcal{E}}(D_\sigma)} F_{\sigma,\epsilon}^n\boldsymbol{u}_\epsilon^{n+\frac12} \\ &\qquad - (\mathrm{div}\boldsymbol{\tau}(\boldsymbol{u}))_\sigma^{n+\frac12} + \left(\frac{\rho_\sigma^n}{\rho_\sigma^{n-1}}\right)^{\frac12}(\boldsymbol{\nabla}p)_\sigma^n = 0, \qquad \sigma\in\mathcal{E}_{\rm int}. \end{aligned} \tag{5.6c}$$

Correction step – Find $(\boldsymbol{u}_\sigma^{n+1})_{\sigma\in\mathcal{E}_{\rm int}}$ and $(p_K^{n+1})_{K\in\mathcal{M}}$ such that:

$$\frac{1}{\delta t}\rho_\sigma^n(\boldsymbol{u}_\sigma^{n+1} - \boldsymbol{u}_\sigma^{n+\frac12}) + (\boldsymbol{\nabla}p)_\sigma^{n+1} - \left(\frac{\rho_\sigma^n}{\rho_\sigma^{n-1}}\right)^{\frac12}(\boldsymbol{\nabla}p)_\sigma^n = 0, \qquad \sigma\in\mathcal{E}_{\rm int}, \tag{5.6d}$$

$$\frac{1}{\delta t}(\rho_K^{n+1} - \rho_K^n) + \frac{1}{|K|}\sum_{\sigma\in\mathcal{E}(K)} F_{K,\sigma}^{n+1} = 0, \qquad K\in\mathcal{M}. \tag{5.6e}$$

In equations (5.6a) and (5.6c), the time level of the density in the time derivative term is shifted with respect to usual formulations; this is due to the fact that the mass balance of the current time step is not solved at this stage and we want to recover the structure which yields a monotone convection operator [15], in (5.6a), or a kinetic preserving operator, as built in the present paper, in (5.6c). For the

face value of the temperature in the convection term, we use an explicit MUSCL-like discretization [21] using an algebraic limitation procedure which ensures the operator monotonicity without any slope reconstruction (so is able to cope with any mesh geometry, which is convenient here). The discretization of the diffusion term is implicit, and performed with a variant of the so-called SUSHI scheme using only the cell-centered variables [21]; if the velocity is prescribed to zero on the whole boundary (or, more precisely speaking, in the absence of energy convection flux entering the domain, as in the test presented in Section 5.3 below), Dirichlet boundary conditions for the temperature are seen, at the discrete level, by the expression of this operator. Note that this scheme is linear and, as all such schemes, preserves the bounds of the unknowns only under restrictive assumptions for the mesh, which are not satisfied by locally refined meshes used here; however, no spurious under- or over-shoots are observed in the computations performed here. The convection term used for the velocity components is defined in Section 3.2. Similarly, the diffusion term is obtained by the standard finite element Galerkin procedure with the shape functions introduced in Section 3.1. Equation (5.6e) is a discretization of the mass balance over the primal mesh, and $F_{K,\sigma}^{n+1}$ stands for the mass flux across σ outward K. On the primal mesh faces, $F_{K,\sigma}^{n+1}$ is given by:

$$F_{K,\sigma}^{n+1} = |\sigma|\ \widehat{\rho}_\sigma^{n+1}\ \boldsymbol{u}_\sigma^{n+1} \cdot \boldsymbol{n}_{K,\sigma}, \qquad \sigma \in \mathcal{E},$$

where $\widehat{\rho}_\sigma^{n+1}$ stands for an approximation of the density at the face σ. Note that, since the density is not an unknown except for the computation of ρ^0 in the initialisation step, we do not need that the discrete mass balance equation ensures its positivity, and any reasonable approximation may be used. Here, we choose a centered approximation at the internal faces of the domain (more precisely speaking, for $n \geq 0$, we compute $\widehat{\rho}_\sigma^{n+1}$ as the mean value of its approximation at the two neighbour cells of σ); for the computation of ρ^0, we use an upwind scheme. The pressure gradient is built as the dual operator of the discrete divergence, itself expressed from the already defined approximation of $\mathrm{div}(\rho\boldsymbol{u})$ by considering that the density is everywhere equal to 1. For $k = n,\ n+1$,

$$(\boldsymbol{\nabla} p)_\sigma^k = \frac{|\sigma|}{|D_\sigma|}(p_L^k - p_K^k)\,\boldsymbol{n}_{K,\sigma}, \quad \forall \sigma \in \mathcal{E}_{\mathrm{int}},\ \sigma = K|L.$$

Finally, the "re-normalization" coefficient which multiplies the pressure gradient ensures that the scheme satisfies a discrete kinetic energy balance (see [10, Appendix A]); it may be seen as a substitute to the additional elliptic problem for the pressure introduced in [11] (and, indeed, the renormalization used here coincides with the results of this technique for one-dimensional problems).

Besides the work in [11], we refer to [17, 18] for another schemes for the solution of System (5.1) together with a benchmark on a problem similar to the one addressed in Section 5.3.

5.2. **A stationary incompressible flow**

We first assess the behavior of the proposed numerical scheme on an exact analytical solution to the stationary incompressible Navier-Stokes equations. The scheme for this problem is derived from System (5.6) by replacing the equation of state by $\rho = 1$ and solving only (5.6c)-(5.6e). The computed flow is known as the Kovasznay flow [14]; the velocity and pressure fields are given by:

$$\boldsymbol{u} = \begin{bmatrix} 1 - e^{\lambda x}\,\cos(2\pi y) \\ \dfrac{\lambda}{2\pi}\, e^{\lambda x}\,\sin(2\pi y) \end{bmatrix}, \quad p = \frac{1}{2}\,(1 - e^{2\lambda x}), \quad \lambda = \frac{1}{2\mu} - \big(\frac{1}{4\mu^2} + 4\pi^2\big)^{1/2},$$

where μ stands for the viscosity of the flow, taken here as $\mu = 1/40$. The computational domain is $\Omega = (-0.5, 1) \times (-0.5, 1.5)$. The mesh is built from a regular $n \times n$ grid, where we refine the sub-domain $\Omega_f = (-0.5, 0.5) \times (-0.5, 0.5) \cup (0.5, 1) \times (0.5, 1.5)$ by splitting each (square) cell included in Ω_f in four sub-squares. The solution is computed by the projection scheme, by letting a computed fictitious

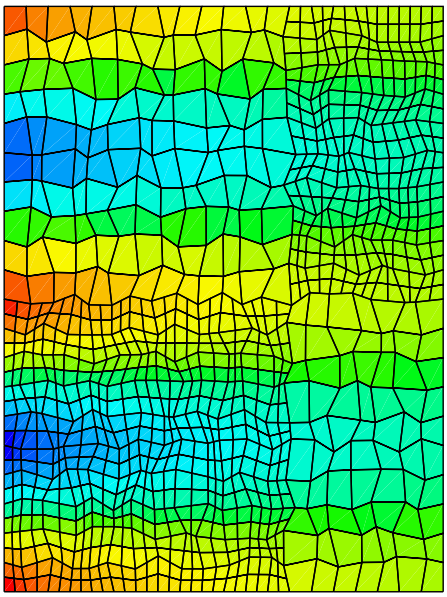

Figure 5. The unstructured mesh built by perturbation of the 20×20 uniform grid. The background is coloured as a function of the first component of the velocity.

transient tend to the desired steady state. Boundary conditions are given by the analytical solution. The obtained numerical errors for various values of n are gathered in the following table, where $\boldsymbol{u}_{\text{exact}}$ and p_{exact} stand for the exact velocity and pressure, respectively.

n	$\|\boldsymbol{u} - \boldsymbol{u}_{\text{exact}}\|_{\mathrm{L}^2(\Omega)^d}$	$\|p - p_{\text{exact}}\|_{\mathrm{L}^2(\Omega)}$
20	0.0384	0.0334
40	0.00825	0.0158
80	0.00211	0.00782
160	0.000544	0.00390

The observed order of convergence (in L^2-norm) is approximately 2 for the velocity and 1 for the pressure.

We now confirm this behaviour on unstructured grids, which are obtained as follows. First, we perturb the 20×20 uniform grid, by moving each internal vertex of the mesh to a random position on a circle centered on its initial location and the radius of which is equal to 0.3 times the smallest distance between the considered vertex and its neighbours (so, for the specific unperturbed mesh used here, 1.5/20). Secondly, we build 3 refined meshes, by splitting each cell in 2, 4 and 8 respectively; by this process, the deviation from a parallelogram of each cell is divided by the same ratio, which ensures optimal convergence properties for the parametric version of the Rannacher-Turek element (see Remark 4.4). Finally, we apply local refinement to the same zones as previously. The coarsest of the obtained four meshes is plotted on Figure 5.

The obtained numerical errors are given in the following table. The orders of convergence are the same as in the uniform case.

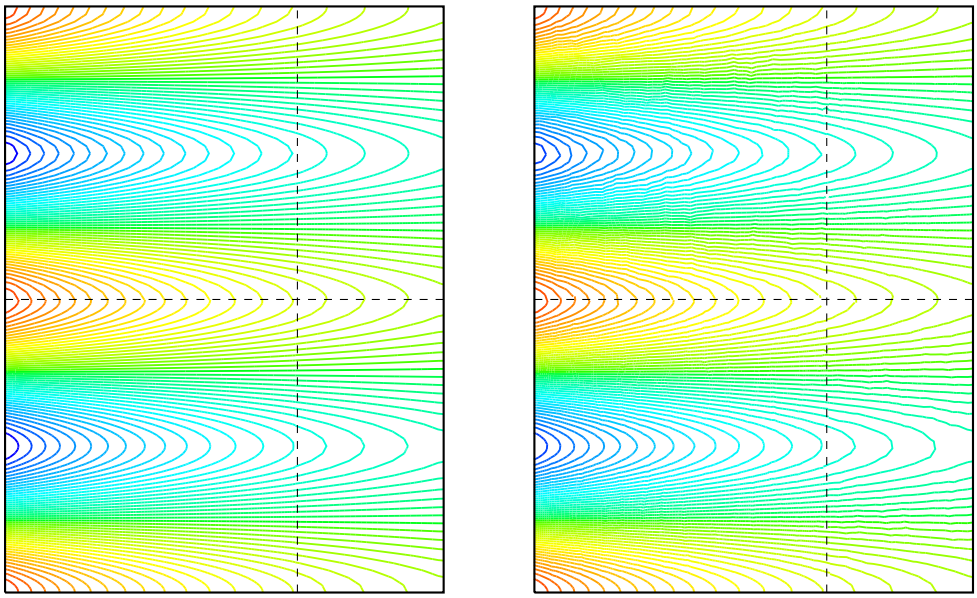

FIGURE 6. Contour lines of the field $\boldsymbol{u}_1$: 80×80 uniform grid (left) and perturbed mesh (right) built by perturbation of the 80×80 grid. The dashed lines materialize the boundary of the refined area (bottom-left and top-right sub-domains).

n	$\|\boldsymbol{u} - \boldsymbol{u}_{\text{exact}}\|_{\mathrm{L}^2(\Omega)^d}$	$\|p - p_{\text{exact}}\|_{\mathrm{L}^2(\Omega)}$
20	0.0617	0.0406
40	0.0119	0.0179
80	0.00281	0.0087
160	0.000718	0.0043

The contour lines of the first component of the velocity are drawn on Figure 6, for both meshes obtained from the 80×80 uniform grid. We may check that no spurious perturbation appears along the lines separating the refined and non-refined parts of the computational domain (in other words, the lines composed by the union of the faces including a hanging node). A careful examination is needed to observe that, as expected, contour lines are slightly more irregular in the unstructured case.

5.3. **Low-Mach buoyant flows**

We now address a natural convection flow governed by the low Mach number asymptotic model (5.1), which falls into the class of differentially heated cavity problems. The computational domain is $\Omega = (0, L)^2$, the velocity and temperature are prescribed on the whole boundary; the velocity is set to zero and the temperature is given by:

$$\vartheta(\boldsymbol{x}) = \frac{L - x_1}{L}\,\vartheta_h + \frac{x_1}{L}\,\vartheta_c, \quad \vartheta_h = (1+\varepsilon)\,\vartheta_0,\ \vartheta_c = (1-\varepsilon)\vartheta_0,$$

with $\vartheta_0 = 600$ and $\epsilon = 0.6$. The left and right vertical boundaries are thus set at a constant (hot and cold, *i.e.* ϑ_h and ϑ_c, respectively) temperature, while this latter varies linearly along the horizontal boundaries, from ϑ_h at $x_1 = 0$ to ϑ_c at $x_1 = L$. Variations of temperature are too large for the Boussinesq approximation of System (5.1) to be valid [17].

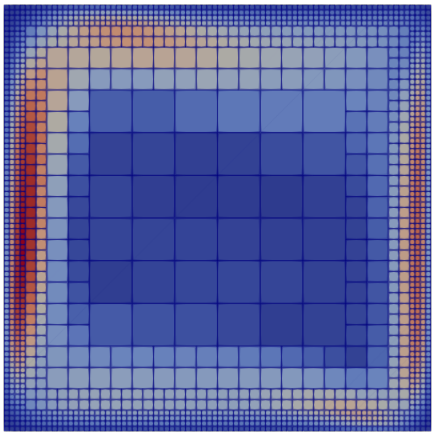

Figure 7. Typical (coarse) mesh. The background is coloured as a function of the norm of the velocity ($\|\boldsymbol{u}\| \in (0,\ 0.25)$). The localization of the refined zones does not exactly match the text specifications because the initial mesh is too coarse; the obtained mesh is third times refined near the boundary and the software ensures that coarse faces only includes two fine ones (*i.e.* there in no interface between ℓ_1 and ℓ_2 times refined zones with $|\ell_1 - \ell_2| > 1$).

The initial thermodynamical pressure and temperature are set to $P_{th}(0) = 101325$ and $\vartheta(\boldsymbol{x}, 0) = \vartheta_0,\ \forall \boldsymbol{x} \in \Omega$, and the fluid is supposed to be initially at rest.

A dimensional analysis shows that the flow is governed by two non-dimensional numbers, namely the Prandtl and the Rayleigh numbers, defined respectively by:

$$\mathrm{Pr} = \frac{\mu\, c_p}{\lambda}, \qquad \mathrm{Ra} = \frac{\rho_0^2\, c_p\, g\, (\vartheta_h - \vartheta_c)\, L^3}{\mu\, \lambda\, \vartheta_0}.$$

For the practical application performed here, we choose $g = 9.81$ and physical properties close to those of the air: $\mu = 1.68\, 10^{-5}$, $c_p = \gamma R/(\gamma - 1)$, with $R = 287$. The Prandtl number is $\mathrm{Pr} = 0.71$, which allows to compute the thermal diffusion λ, and the size of the domain L will be determined as a function of the chosen Rayleigh number.

A stability analysis of this natural convection flow is given in [26]. It shows that the flow reaches a steady state up to a critical value of the Rayleigh number approximately equal to $\mathrm{Ra} = 2.1\, 10^6$. Beyond this value, the flow remains time-dependent, with traveling waves along the boundaries, issued from exiting corners of the vertical boundary layers. Our aim here is to assess the capability of the proposed scheme to confirm this behaviour in the non-Boussinesq approach; an accurate determination of the critical Rayleigh number is however beyond the scope of this section.

The mesh used for this study is built as follows: we start from a 80×80 uniform grid, perform a first refinement step splitting each cell located in $\Omega \setminus (0.15\, L,\ 0.85\, L)^2$, a second one by subdividing once-again the cells in $\Omega \setminus (0.1\, L,\ 0.9\, L)^2$, and, finally, a third one by splitting the resulting cells in $\Omega \setminus (0.05\, L,\ 0.95\, L)^2$; at each refinement step, the cells are cut in 4, so *in fine* the characteristic sizes of the cells near the boundary are $\delta x_1 = \delta x_2 = L/640$. A mesh obtained by the same process from the 10×10 uniform grid is shown on Figure 7. The background color in this figure is the temperature; one can see that steep variations of the solution are concentrated in the boundary layers, which justifies the chosen refinement.

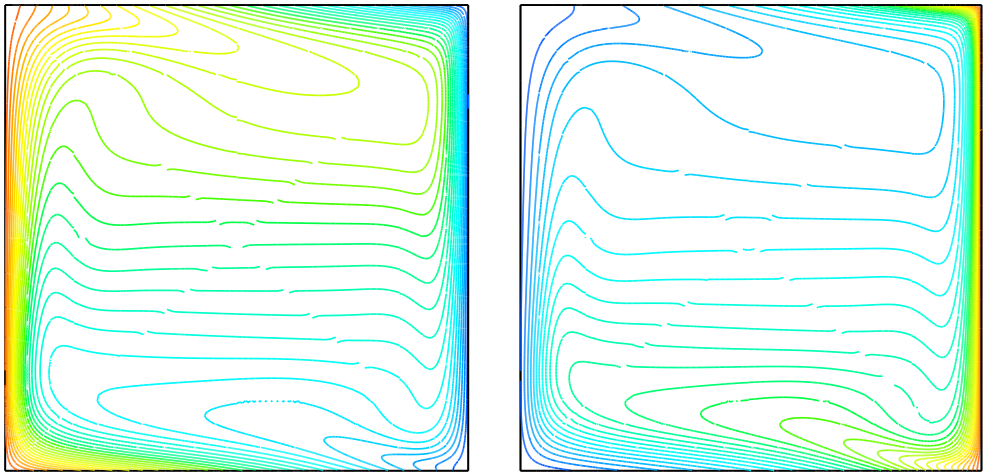

FIGURE 8. Temperature ($\vartheta \in (240,\ 960)$) and density ($\rho \in (0.33,\ 1.32)$) at the steady state, for $Ra = 2\,10^6$.

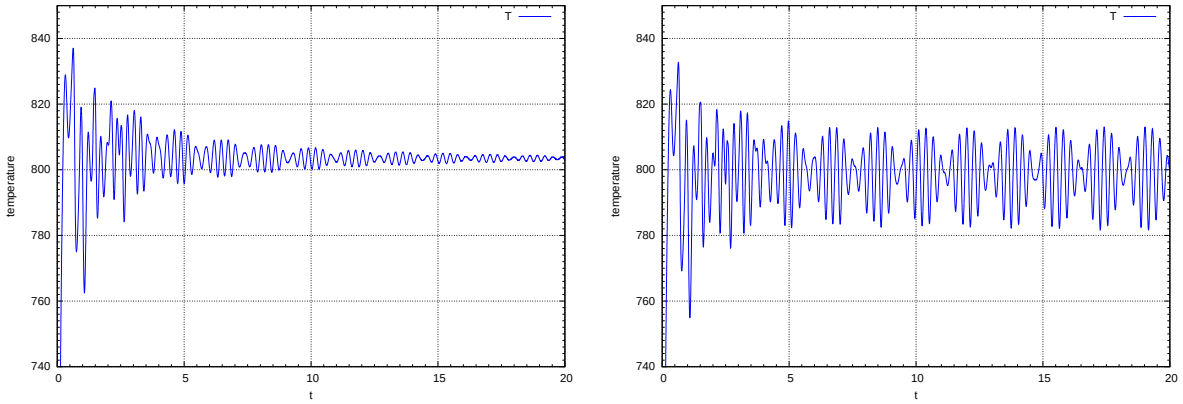

$\mathrm{Ra} = 2\,10^6$ $\mathrm{Ra} = 2.2\,10^6$

FIGURE 9. Temperature as a function of time at the location $\boldsymbol{x} = (0.1\,L,\ 0.92\,L)^t$, for different Rayleigh values.

At $Ra = 2\,10^6$, the flow after 20 time units is stationary (at least approximately, see Figure 9 below). The obtained temperature and density fields are plotted on Figure 8. On can observe that the non-linearity of the equation of state makes that the flow looses its symmetry, and generates steep density gradients at the right boundary.

We then plot the evolution with time of the temperature at the location $\boldsymbol{x} = (0.1\,L,\ 0.92\,L)^t$, for $\mathrm{Ra} = 2\,10^6$ and $\mathrm{Ra} = 2.2\,10^6$. We observe that, for $\mathrm{Ra} = 2\,10^6$, the flow tends to a steady state, while an oscillatory (quasi-periodic) behaviour subsists at $\mathrm{Ra} = 2.2\,10^6$, which is consistent with the value for the critical Rayleigh known under the Boussinesq approximation [26].

Appendix A. Construction of the dual fluxes

A.1. Dual fluxes for non-refined meshes

The system of equations (3.7) has an infinity of solutions, which explains the necessity of the additional constraint (H3). Since (3.7) is linear with respect to the $F_{\sigma,\epsilon}$, $\sigma \in \mathcal{E}(K)$, $\epsilon \in \tilde{\mathcal{E}}(D_\sigma)$, $\epsilon \subset K$, a solution of (3.7) may thus be expressed as:

$$F_{\sigma,\epsilon} = \sum_{\sigma' \in \mathcal{E}(K)} (\alpha_K)_\sigma^{\sigma'} \; F_{K,\sigma'}, \qquad \sigma \in \mathcal{E}(K), \epsilon \in \tilde{\mathcal{E}}(D_\sigma) \text{ and } \epsilon \subset K,$$

and (H3) is equivalent to requiring bounded coefficients $((\alpha_K)_\sigma^{\sigma'})_{\sigma,\sigma' \in \mathcal{E}(K)}$. In addition, since $\xi_K^\sigma = 1/(2d)$ for all $K \in \mathcal{M}$ and $\sigma \in \mathcal{E}(K)$ (we recall that the mesh is not refined here), system (3.7) is completely independent from the cell K under consideration. We may thus consider a particular geometry for K, let us say $K = (0,1)^d$, and find an expression for the coefficients $((\alpha_K)_\sigma^{\sigma'})_{\sigma,\sigma' \in \mathcal{E}(K)}$ which we will apply to all the cells, thus automatically satisfying the constraint (H3). A technique for this computation is described in [1, Section 3.2]. The idea is to build a momentum field $\boldsymbol{w}$ with a constant divergence and such that

$$\int_\sigma \boldsymbol{w} \cdot \boldsymbol{n}_{K,\sigma} = F_{K,\sigma}, \qquad \forall \sigma \in \mathcal{E}(K).$$

Then, an easy computation shows that the following fluxes satisfy (3.7):

$$F_{\sigma,\epsilon} = \int_\epsilon \boldsymbol{w} \cdot \boldsymbol{n}_{\sigma,\epsilon}. \tag{A.1}$$

Two-dimensional case - For $d = 2$, using the notations introduced in Figure 10, such a momentum field $\boldsymbol{w}$ is given by:

$$\boldsymbol{w}(x,y) = \begin{bmatrix} (1-x)\,(-F_{\mathrm{W}}) + x\,F_{\mathrm{E}} \\ (1-y)\,(-F_{\mathrm{S}}) + y\,F_{\mathrm{N}} \end{bmatrix}.$$

Using (A.1), we obtain:

$$F_{\sigma,\epsilon} = \alpha_{\mathrm{W}} F_{\mathrm{W}} + \alpha_{\mathrm{E}} F_{\mathrm{E}} + \alpha_{\mathrm{S}} F_{\mathrm{S}} + \alpha_{\mathrm{N}} F_{\mathrm{N}},$$

with the coefficients α_{W}, α_{E}, α_{S} and α_{N} given in table 1. The notation $F_{\mathrm{W|S}}$ for the dual flux means that one calculates the flux from the western (W) to the southern (S) region with this orientation.

$F_{\sigma,\epsilon}$	α_{W}	α_{E}	α_{S}	α_{N}
$F_{\mathrm{W\|S}}$	$-3/8$	$1/8$	$3/8$	$-1/8$
$F_{\mathrm{S\|E}}$	$-1/8$	$3/8$	$-3/8$	$1/8$
$F_{\mathrm{E\|N}}$	$1/8$	$-3/8$	$-1/8$	$3/8$
$F_{\mathrm{N\|W}}$	$3/8$	$-1/8$	$1/8$	$-3/8$

Table 1. Expression of the dual fluxes in 2D.

Three-dimensional case - For $d = 3$, using the notations introduced in Figure 11, we may choose, for the constant divergence momentum field $\boldsymbol{w}$, the following expression:

$$\boldsymbol{w}(x,y,z) = \begin{bmatrix} (1-x)\,(-F_{\mathrm{W}}) + x\,F_{\mathrm{E}} \\ (1-y)\,(-F_{\mathrm{S}}) + y\,F_{\mathrm{N}} \\ (1-z)\,(-F_{\mathrm{B}}) + z\,F_{\mathrm{F}} \end{bmatrix}.$$

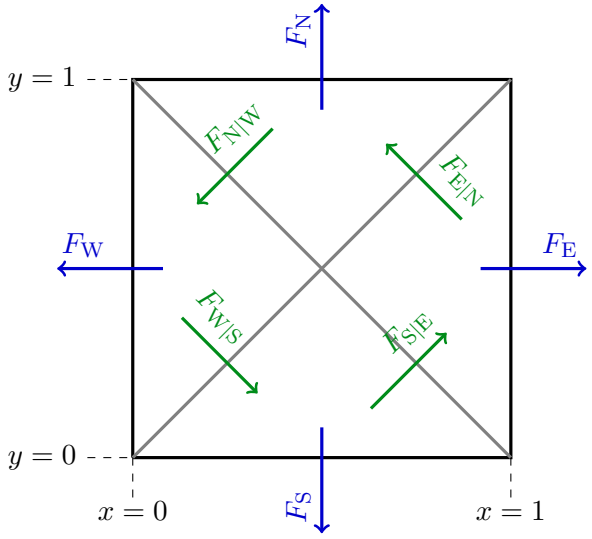

FIGURE 10. Notations for the primal and dual fluxes in 2D.

The dual fluxes may be expressed as linear combinations of the primal ones:

$$F_{\sigma,\epsilon} = \alpha_{\mathrm{W}} F_{\mathrm{W}} + \alpha_{\mathrm{E}} F_{\mathrm{E}} + \alpha_{\mathrm{S}} F_{\mathrm{S}} + \alpha_{\mathrm{N}} F_{\mathrm{N}} + \alpha_{\mathrm{B}} F_{\mathrm{B}} + \alpha_{\mathrm{F}} F_{\mathrm{F}}$$

where the coefficients α_{W}, α_{E}, α_{S}, α_{N}, α_{B}, α_{F} are given in table 2.

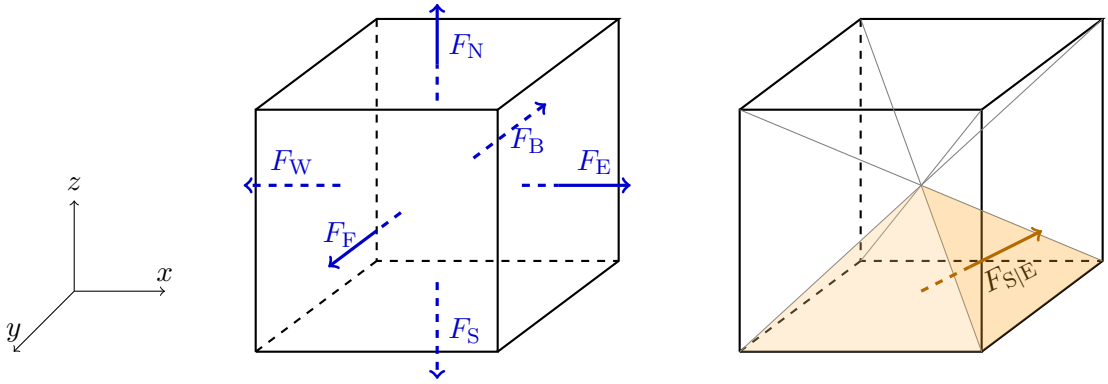

FIGURE 11. Notations for the primal and dual fluxes in 3D.

A.2. **Dual fluxes for refined meshes**

Here again, we may restrict the computation to square ($d = 2$) or cubic ($d = 3$) cells.

Two-dimensional case - In 2D, if a primal cell is surrounded with four refined cells, the half-diamond cells are obtained by splitting the cell in four sub-squares, each one being split in two triangles. Hence, eight dual fluxes must be computed; if some of the neighboring cells are not refined, one uses a *coarsening* procedure, which just consists in keeping the fluxes associated to the fully refined cases on existing dual faces and disregarding the other ones (the mass balance still holds by conservativity).

$F_{\sigma,\epsilon}$	α_{W}	α_{E}	α_{S}	α_{N}	α_{B}	α_{F}
$F_{\mathrm{F\|S}}$	0	0	5/24	−1/24	1/24	−5/24
$F_{\mathrm{S\|B}}$	0	0	−5/24	1/24	5/24	−1/24
$F_{\mathrm{B\|N}}$	0	0	−1/24	5/24	−5/24	1/24
$F_{\mathrm{N\|F}}$	0	0	1/24	−5/24	−1/24	5/24
$F_{\mathrm{W\|S}}$	− 5/24	1/24	5/24	−1/24	0	0
$F_{\mathrm{S\|E}}$	− 1/24	5/24	−5/24	1/24	0	0
$F_{\mathrm{E\|N}}$	1/24	−5/24	−1/24	5/24	0	0
$F_{\mathrm{N\|W}}$	5/24	−1/24	1/24	−5/24	0	0
$F_{\mathrm{F\|E}}$	− 1/24	5/24	0	0	1/24	−5/24
$F_{\mathrm{E\|B}}$	1/24	−5/24	0	0	5/24	−1/24
$F_{\mathrm{B\|W}}$	5/24	−1/24	0	0	−5/24	1/24
$F_{\mathrm{W\|F}}$	− 5/24	1/24	0	0	−1/24	5/24

Table 2. Expression of the dual fluxes in 3D.

We use the notations of Figure 12, so that $(F_{K,\sigma})_{\sigma\in\mathcal{E}(K)}$ denoted here by F_i $(4 \le i \le 11)$ and $F_{\sigma,\epsilon},\ \sigma \in \mathcal{E}(K), \epsilon \subset K$ denoted here by $\widetilde{F}_i$ $(0 \le i \le 7)$. We begin with computing the dual fluxes across the four sub-squares faces ($\widetilde{F}_i$ $(4 \le i \le 7)$, red color in Figure 12) so that (3.7) holds. The linear system to solve has a one dimensional kernel and a particular solution satisfying $(H3)$ is given by:

$$
\begin{aligned}
\widetilde{F}_4 &= \frac{3}{8}\,(F_5 + F_6 \ - F_{11} - F_4\ ) \ + \ \frac{1}{8}\,(F_7 + F_8 \ - F_9 \ - F_{10}),\\
\widetilde{F}_5 &= \frac{3}{8}\,(F_7 + F_8 \ - F_5 \ - F_6\ ) \ + \ \frac{1}{8}\,(F_9 + F_{10} - F_{11} - F_4),\\
\widetilde{F}_6 &= \frac{3}{8}\,(F_9 + F_{10} - F_7 \ - F_8\ ) \ + \ \frac{1}{8}\,(F_4 + F_{11} - F_5 \ - F_6),\\
\widetilde{F}_7 &= \frac{3}{8}\,(F_4 + F_{11} - F_9 \ - F_{10}) \ + \ \frac{1}{8}\,(F_5 + F_6 \ - F_7 \ - F_8).
\end{aligned}
$$

Then, the dual fluxes across the diagonal faces $\bar{F}_i$ $(0 \le i \le 3)$ (green color in Figure 12) are computed by isolating the sub-squares and applying the procedure described above for the non-refined case. For instance, $\bar{F}_1 = F_{E|N} - F_{W|S}$, where $F_E := F_7$, $F_N := F_8$, $F_W := \widetilde{F}_6$, and $F_S = -\widetilde{F}_5$.

Three-dimensional case - The procedure is the same as in the 2D-case. The first step consists in splitting the cube in eight sub-cubes and computing the dual fluxes across the faces of these sub-cubes. The formula of one of these intermediate fluxes $\widetilde{F}$ (see Figure 13) is given by:

$$
\begin{aligned}
24\ \widetilde{F} \ &= \ 7\ (\ F_{14} + F_{21} + F_{27}\ ) \ - \ 7\ (\ F_{15} + F_{19} + F_{25}\ )\\
&+ \ 2\ (\ F_7 \ + F_{20} + F_{26}\ ) \ - \ 2\ (\ F_6 \ + F_{18} + F_{24}\ )\\
&+ \ 2\ (\ F_{11} + F_{16} + F_{29}\ ) \ - \ 2\ (\ F_{13} + F_{17} + F_{23}\ )\\
&+ \quad (\ F_9 \ + F_{10} + F_{28}\ ) \ - \quad (\ F_8 \ + F_{12} + F_{22}\ ).
\end{aligned}
$$

The computation of the other fluxes across the faces separating two sub-cubes is deduced by permutations of the indices.

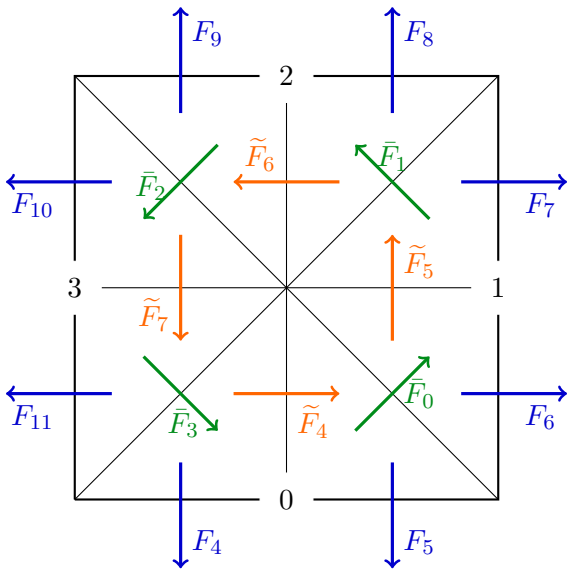

FIGURE 12. Dual fluxes for the neighboring cell of refined cells (2D case).

In the second step, each sub-cube is split in 3 half-diamonds of equal volumes. One obtains 24 half-diamonds and 48 internal half-diamond faces of two possible types (see Figure 15). The dual fluxes across these faces are obtained by isolating the sub-cubes and applying the procedure described above for the non-refined case, consisting in integrating the momentum field $\boldsymbol{w}$ over the faces of interest; the resulting expressions are gven on Figure 15.

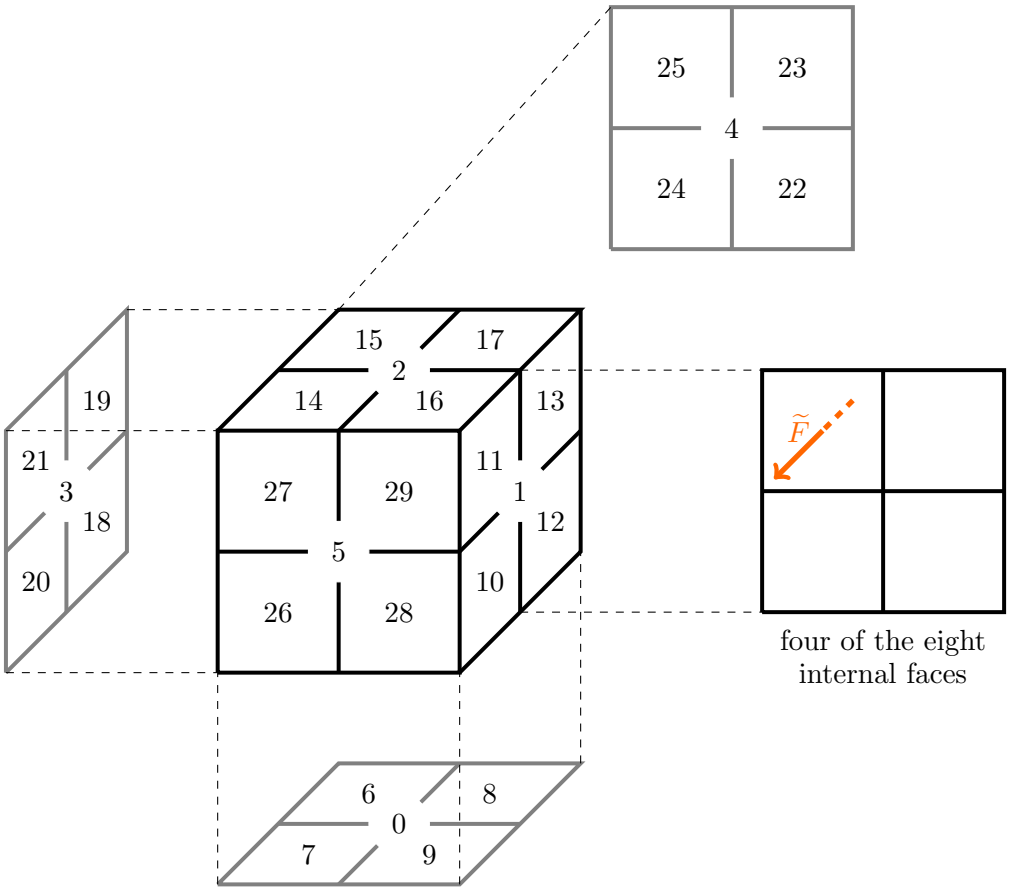

Figure 13. Intermediate dual fluxes for the neighboring cell of refined cells (3D case).

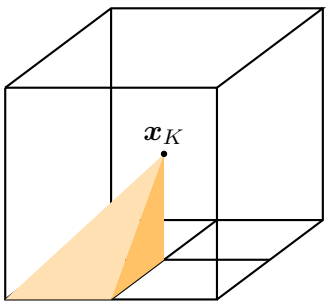

Figure 14. Two possible types of internal half-diamond faces (3D case).

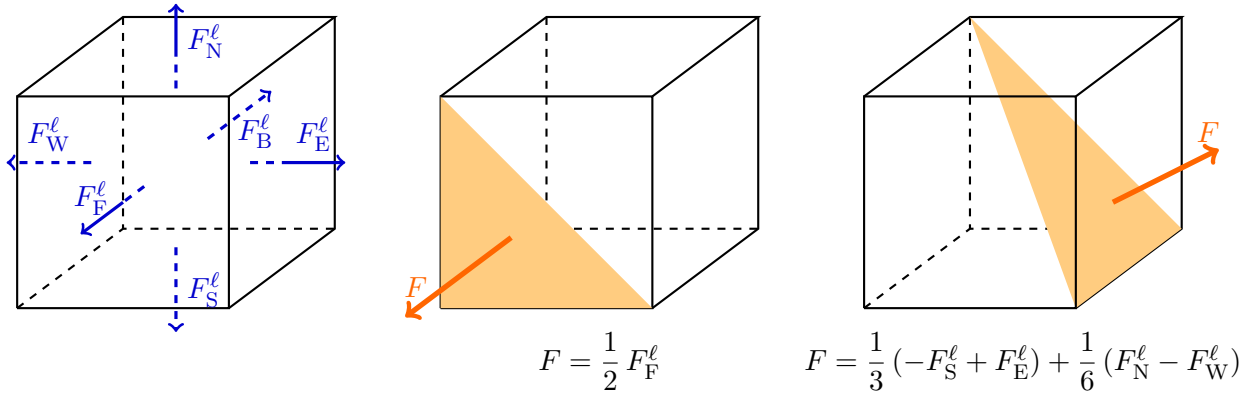

FIGURE 15. Expression of the fluxes for the two possible types of internal half-diamond faces (3D case).

Appendix B. Splitting of hexahedra with plane faces

We mention in Remark 4.4 that splitting an hexahedra having only plane faces may make some curved faces appear. This assertion being rather non intuitive, we give here an example of this phenomena. Let us begin with a volume having three quadrangular faces and two triangular faces, as sketched on Figure 16. With te notations of the figure, let:

$$A = \begin{bmatrix}0\\0\\0\end{bmatrix}, \quad B = \begin{bmatrix}1\\0\\0\end{bmatrix}, \quad C = \begin{bmatrix}2\\2\\0\end{bmatrix}, \quad D = \begin{bmatrix}0\\1\\0\end{bmatrix}, \quad E = \begin{bmatrix}0\\1/2\\1/2\end{bmatrix}, \quad F = \begin{bmatrix}2\\1\\1\end{bmatrix}.$$

We get:

$$EF = 2\ AB + AE = DC - DE,$$

so both the faces $ABFE$ and $DCFE$ are plane, while the face $ABCD$ is included in the plane $x_3 = 0$ and the triangular faces are obviously planes. Let A', B', C' and D' be the mid point of the segments AE, BF, CF and DE respectively. Then

$$\det(A'B', A'D', B'C') = 1,$$

so the points A', B', C' and D' are not in the same plane. Let us now cut this volume by a plane spanned by $\{EF,\ \boldsymbol{e}^{(2)}\}$, with $\boldsymbol{e}^{(2)}$ the second vector of the canonical base of $\mathbb{R}^3$, and sufficiently close to EF. This operation yields an hexahedra having only plane faces. By continuity, it is clear that we may have $\det(A'B', A'D', B'C') \neq 0$, with A', B', C' and D' being the mid point of the new edges issued from A, B, C and D respectively and not included in the $x_3 = 0$ plane.

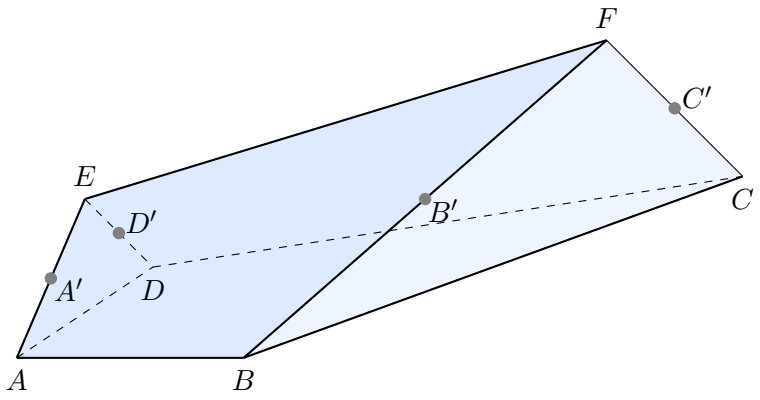

Figure 16. Notations for Appendix B.

Bibliography

[1] G. Ansanay-Alex, F. Babik, J.-C. Latché, and D. Vola. An L^2-stable approximation of the Navier-Stokes convection operator for low-order non-conforming finite elements. *International Journal for Numerical Methods in Fluids*, 66:555–580, 2011.

[2] M. Bebendorf. A note on the Poincaré inequality for convex domains. *Journal for Analysis and its Applications*, 22:751–756, 2003.

[3] R. Becker and S. Mao. Quasi-optimality of adaptative nonconforming finite element methods for the Stokes equations. *SIAM Journal on Numerical Analysis*, 49:970–991, 2011.

[4] F. Boyer, F. Dardalhon, C. Lapuerta, and J.-C. Latché. Stability of a Crank-Nicolson pressure correction scheme based on staggered discretizations. *International Journal for Numerical Methods in Fluids*, 74:34–58, 2014.

[5] CALIF^{3}S. A software components library for the computation of reactive turbulent flows. `https://gforge.irsn.fr/gf/project/isis`.

[6] A.J. Chorin. Numerical solution of the Navier-Stokes equations. *Mathematics of Computation*, 22:745–762, 1968.

[7] P. G. Ciarlet. Basic error estimates for elliptic problems. In P. Ciarlet and J.L. Lions, editors, *Handbook of Numerical Analysis, Volume II*, pages 17–351. North Holland, 1991.

[8] R. Eymard, R. Herbin, J.-C. Latché, and B. Piar. Convergence analysis of a locally stabilized collocated finite volume scheme for incompressible flows. *Mathematical Modelling and Numerical Analysis*, 43:889–927, 2009.

[9] T. Gallouët, L. Gastaldo, R. Herbin, and J.-C. Latché. An unconditionally stable pressure correction scheme for compressible barotropic Navier-Stokes equations. *Mathematical Modelling and Numerical Analysis*, 42:303–331, 2008.

[10] D. Grapsas, R. Herbin, W. Kheriji, and J.-C. Latché. An unconditionally stable staggered pressure correction scheme for the compressible Navier-Stokes equations. *SMAI Journal of Computational Mathematics*, 2:51–97, 2016.

[11] J.-L. Guermond and L. Quartapelle. On the approximation of the unsteady Navier-Stokes equations by finite element projection methods. *Numerische Mathematik*, 80:207–238, 1998.

[12] J.L. Guermond, P. Minev, and J. Shen. An overview of projection methods for incompressible flows. *Computer Methods in Applied Mechanics and Engineering*, 195:6011–6045, 2006.

[13] R. Herbin, W. Kheriji, and J.-C. Latché. On some implicit and semi-implicit staggered schemes for the shallow water and Euler equations. *Mathematical Modelling and Numerical Analysis*, 48:1807–1857, 2014.

[14] L.-I.-G. Kovasznay. Laminar flow behind a two-dimensional grid. *Mathematical Proceedings of the Cambridge Philosophical Society*, 44:[58], 1948.

[15] B. Larrouturou. How to preserve the mass fractions positivity when computing compressible multi-component flows. *Journal of Computational Physics*, 95:59–84, 1991.

[16] J.-C. Latché and K. Saleh. A convergent staggered scheme for variable density incompressible Navier-Stokes equations. *Mathematics of Computation*, 87:581–632, 2018.

[17] P. Le Quéré, C. Weisman, H. Paillère, J. Vierendeels, E. Dick, R. Becker, M. Braack, and J. Locke. Modelling of natural convection flows with large temperature differences: a benchmark problem for low Mach number solvers. Part 1. Reference solutions. *Mathematical Modelling and Numerical Analysis*, 39:609–616, 2005.

[18] P. Le Quéré, C. Weisman, H. Paillère, J. Vierendeels, E. Dick, R. Becker, M. Braack, and J. Locke. Modelling of natural convection flows with large temperature differences: a benchmark problem for low Mach number solvers. Part 2. ????. *Mathematical Modelling and Numerical Analysis*, 39:???, 2005.

[19] A. Majda and J. Sethian. The derivation and numerical solution of the equations for zero Mach number solution. *Combustion Science and Techniques*, 42:185–205, 1985.

[20] L.E. Payne and H.F. Weinberger. An optimal Poincaré-inequality for convex domains. *Archive for Rational Mechanics and Analysis*, 5:286–292, 1960.

[21] L. Piar, F. Babik, R. Herbin, and J.-C. Latché. A formally second order cell centered scheme for convection-diffusion equations on general grids. *International Journal for Numerical Methods in Fluids*, 71:873–890, 2013.

[22] R. Rannacher and S. Turek. Simple nonconforming quadrilateral Stokes element. *Numerical Methods for Partial Differential Equations*, 8:97–111, 1992.

[23] F. Schieweck and L. Tobiska. A nonconforming finite element method of upstream type applied to the stationary Navier-Stokes equation. *Mathematical Modelling and Numerical Analysis*, 23:627–647, 1989.

[24] F. Schieweck and L. Tobiska. An optimal order error estimate for an upwind discretization of the Navier-Stokes equations. *Numerical Methods for Partial Differential Equations*, 12:407–421, 1996.

[25] R. Temam. Sur l'approximation de la solution des équations de Navier-Stokes par la méthode des pas fractionnaires II. *Arch. Rat. Mech. Anal.*, 33:377–385, 1969.

[26] S. Xin and P. Le Quéré. Linear stability analyses of natural convection flows in a differentially heated square cavity with conducting horizontal walls. *Physics of Fluids*, 13:2529–2542, 2001.